Bulletin of the Seismological Society of America, Vol. 100, No. 5A, pp. 2196–2218, October 2010, doi: 10.1785/0120090223

Regional Wave Propagation in New England and New York

by Gisela M. Viegas, Laurie G. Baise, and Rachel E. Abercrombie

Abstract We validate and improve 1D velocity models of the two main crustal provinces in the northeastern United States (NEUS), using seismograms from the 20 April 2002 *M* 5 Au Sable Forks earthquake, which is the largest earthquake in the region to be recorded by multiple, recently deployed, good-quality, regional broadband stations. To predict and mitigate the effects of future earthquakes in the northeastern United States, more information is needed regarding both the local earthquake sources and how seismic waves travel through the region. We investigate the source and regional wave propagation for the Au Sable Forks earthquake. The earthquake epicenter is located near the boundary of two distinct geological provinces, the Appalachian (New England) and Grenville (New York). We use a forward-modeling approach to study the waveforms recorded at 16 stations located within 400 km of the epicenter. We generate synthetic seismograms using the frequency–wavenumber method, testing several published models for the two provinces. Several models perform well at low frequencies (<0.1 Hz). We refine these models and generate two alternative 1D crustal models for intermediate frequencies (<1 Hz) of engineering interest. Our new Grenville model performs better than previously published models for all six source-station paths modeled in that province according to goodness of fit statistics: variance reduction and correlation coefficient. Our alternative Appalachian model improves the fit of synthetics to data for five of the ten paths modeled in that province. From the results, we identify two specific sources of wave-field complexities that should be investigated in future studies of earthquake ground motions in NEUS: 3% azimuthal anisotropy in the Appalachian Province and complex wave paths along the boundary between the two provinces.

Introduction

To predict and mitigate the effects of future earthquakes in the northeastern United States (NEUS), we need to know more about both the local earthquake sources and how seismic waves travel through the region. Seismic hazard in NEUS is primarily evaluated using the United States National Seismic Hazard Maps based on probabilistic seismic hazard analysis (PSHA) developed by the United States Geologic Survey (USGS). The PSHA relies on background seismicity and Gutenberg–Richter recurrence models to determine the recurrence of earthquakes (Frankel *et al.*, 1996, 2002; Peterson *et al.*, 2008) and a series of ground motion relations (e.g., Frankel *et al.*, 1996; Toro *et al.*, 1997; Somerville *et al.*, 2001; Silva *et al.*, 2002; Campbell, 2003; Tavakoli and Pezeshk, 2005; Atkinson and Boore, 2006) to determine the ground shaking level for a given earthquake-site pairing. Four of the ground motion relations (Frankel *et al.*, 1996; Toro *et al.*, 1997; Silva *et al.*, 2002; Atkinson and Boore, 2006) rely primarily on stochastic simulations for developing ground motions with stress drop, focal depth, crustal velocity structure, near-site attenuation, and crustal anelastic attenuation as parameters. Two of the ground motion relations (Campbell, 2003; Tavakoli and Pezeshk, 2005) are hybrid empirical models that use western United States data, transformed to imitate central and eastern United States characteristics. The final model (Somerville *et al.*, 2001) uses full waveform simulations and accounts for finite fault rupture for large earthquakes. The aleatory and epistemic uncertainty in the PSHA for NEUS is significant and can greatly influence the earthquake ground motions used in design (Hines *et al.*, 2010). In the next five years, new ground motion prediction equations will be developed as part of the Next Generation Attenuation–East Project (NGA–East) with the intention of reducing uncertainty in ground motion prediction in the central and eastern United States (CEUS). As discussed in every paper on earthquake hazard in the CEUS, as well as the NEUS, ground motion and source models for the regions are limited by the few existing ground-motion recordings. Each earthquake that occurs in the region provides an opportunity for validating and improving models. We use the 2002 Au Sable Forks event to test and improve regional crustal models for NEUS. Although only one of the seven ground motion prediction equations used in the 2008 National Seismic Hazard Maps relies on full waveform simulations, a better understanding of regional sources and wave propagation will be useful to NGA-East researchers, as well as in future efforts to characterize seismic hazard in the NEUS.

Unlike the west coast of the United States, where numerous studies on regional wave propagation have been completed (e.g., Dreger and Helmberger, 1990; Wald and Graves, 1998; Stidham *et al.*, 1999; Olsen, 2000; Pitarka *et al.*, 2004; Kim *et al.*, 2010), investigation of regional wave propagation in NEUS (e.g., Somerville, 1989; Hughes and Luetgert, 1991; Zhao and Helmberger, 1991; Saikia, 1994) is limited due to the lack of large earthquakes and good station coverage. The Au Sable Forks earthquake (M_L 5.3, M 5.0, 20 April 2002) is the largest earthquake to occur in the NEUS since the installation of broadband networks in the region; and, as a result, it provides the first opportunity to investigate wave propagation to multiple broadband stations and to test regional models. The M 5.9 Saguenay (Quebec) earthquake (25 November 1988) was the last moderate earthquake to have occurred in the region. It was recorded at one broadband station (HRV) and at several short-period stations from the Eastern Canadian Telemetered Network (ECTN) within 625 km and has had a significant influence on subsequent regional ground motion studies (Atkinson and Boore, 1995, 1998; Toro *et al.*, 1997). The good-quality ground motions recorded during the Au Sable Forks earthquake at more than 50 modern broadband stations (16 within 400 km) provide a unique opportunity to investigate the source process, regional wave propagation, and ground motions of a moderate earthquake in the region. Atkinson and Sonley (2003) studied the ground motions recorded by the Au Sable Forks earthquake using a variety of spectral methods. They found that the earthquake ground motions are consistent with the prediction of several ground motion relations for eastern North America (ENA) (Atkinson and Boore, 1995; Toro *et al.*, 1997; Somerville *et al.*, 2001; and Campbell, 2003).

The Au Sable Forks earthquake was located near the Champlain Thrust that divides the Appalachian and the Grenville Provinces (see Fig. 1). The Proterozoic crust of the Grenville Province has higher seismic velocities than the Paleozoic accreted terranes of the Appalachian Province (e.g., Taylor *et al.*, 1980; Hughes and Luetgert, 1991; Musacchio *et al.*, 1997). Because the Au Sable Forks earthquake epicenter is located near the boundary of the two provinces,

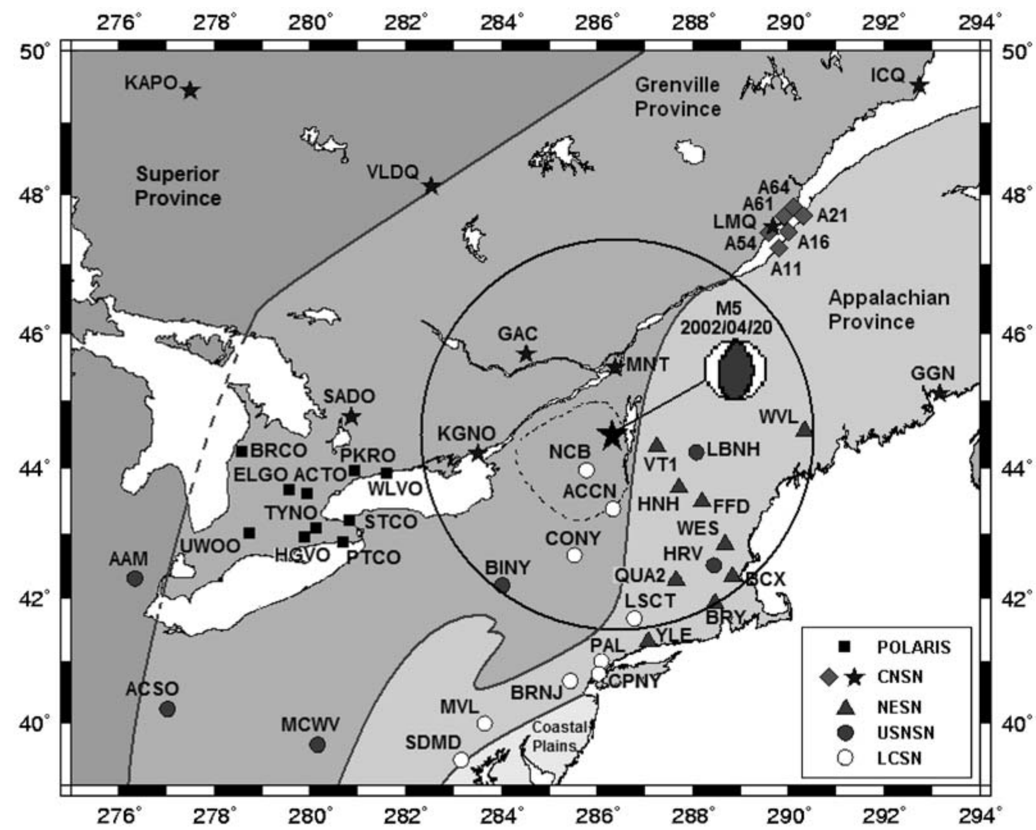

Figure 1. Broadband stations in operation in eastern North America since 2002. The focal mechanism and epicenter (star) of the 2002 Au Sable Fork earthquake are indicated. The circle with an approximate radius of 400 km constricts the stations used in this study. The Appalachian and Grenville Provinces are labeled and differentiated by different shades of gray, and the approximate location of the boundary between the two provinces is indicated by a solid line. The dashed line indicates the contour of the Central Granulite Terrane within the Grenville Province.

we can use independent crustal models for each province. The Appalachian Province is to the east of the epicenter and underlies New England, whereas the Grenville Province underlies New York State, west of the epicenter. By validating more regionally specific crustal models, we can potentially provide guidance for future seismic hazard studies in NEUS and specifically help provide more information on seismic wave propagation in NEUS.

We investigate the regional wave propagation from the Au Sable Forks earthquake in both the Appalachian and Grenville Provinces. A few 1D velocity models exist in the literature for the two provinces (regional crustal models adopted by the Lamont–Doherty Cooperative Seismographic Network (LCSN); Somerville, 1989; Hughes and Luetgert, 1991; Zhao and Helmberger, 1991; Saikia, 1994; Helmberger *et al.*, 1992; and Somerville *et al.*, 2001). The first goal of this research is to test existing 1D velocity models by generating synthetic seismograms and comparing them to the Au Sable Forks recorded ground motions and validate these models based on their performance in terms of goodness of fit. The second goal is to improve the best-fitting existing model for each geological province by iteratively altering the crustal model to better match the observed Au Sable Forks ground motions. Accurate 1D models are fundamental for seismic hazard studies through their role in source inversions, ground motion prediction equations, and for subsequent 2D and 3D regional wave propagation studies. We use the frequency–wavenumber method for wave propagation and compare synthetic and recorded waveforms using two goodness of fit measures: variance reduction and correlation coefficient. Variance reduction provides an estimate of amplitude fit but can be misleading when a time lag exists; therefore, the correlation coefficient is used to evaluate shape and identify time lags. We analyze the records up to frequencies of 1 Hz to address frequencies of engineering interest, using the forward-modeling approach of Dreger and Helmberger (1990). Following this method, we evaluate the sensitivity of the synthetic wave field to perturbations of the crustal-layer thicknesses and velocities, identify which crustal reflectors are responsible for which waveform features, and improve the regional model. In addition to the published 1D velocity models, numerous seismic reflection and wide-angle refraction analyses of the region provide additional information on crustal structure and velocities (Hughes and Luetgert, 1991 and 1992; Hughes *et al.*, 1993; Musacchio *et al.*, 1997). Because we know that the 1D velocity models do not capture the actual crustal structure, the third goal is to identify observed misfits in the data not captured by the regional 1D velocity models and to try to understand where the 1D approximation is not appropriate and where crustal heterogeneity and complexity affects waveforms in NEUS.

We begin by describing the regional geology, the existing published 1D velocity models used in this study, and the Au Sable Forks earthquake. Next, we describe the procedure to generate the synthetic seismograms, including the determination of the earthquake source parameters, and test the existing models. Finally, we perform a sensitivity study on existing crustal models and then incrementally adjust crustal models to produce synthetics for comparison to the observed ground motions of the Au Sable Forks earthquake. Through this effort, we provide recommendations on appropriate 1D models for the Appalachian and Grenville Provinces in the NEUS and identify possible crustal complexities and azimuthal anisotropy that merit further study.

Geological Setting

The NEUS is characterized by two distinct lithologies: the Precambrian Grenville Province on the west, and the Paleozoic Appalachian Province on the east, that overthrusts the Grenvillian basement (Seeber *et al.*, 2002). The boundary between the two regions, the Taconic suture, is visible at the surface from the Labrador Sea to Alabama and strikes approximately north-northeast–south-southwest (Wheeler, 1995). In New England, the boundary is expressed as the Grenvillian Ramp, a 20 km deep, east-dipping fault (Musacchio *et al.*, 1997) which surfaces as the Champlain Thrust. The surface boundary line between the two provinces is shown in Figure 1. Differences in crustal compositions of the two provinces reflect different formation processes and ages. The Grenville orogeny (1.3 Ga to 1.0 Ga ago) produced metamorphic and igneous rocks (Musacchio *et al.*, 1997) associated with the collision of Laurentia (eastern North America) with Amazonia (western South America) and the subsequent formation of the supercontinent Rodinia (Levin, 2006). Grenvillian rocks are mostly granulites-grade metasediments intruded by anorthosites (Hughes and Luetgert, 1992). The epicentral region is located on the east side of the Central Granulite Terrane (Adirondack massif), close to a large anorthosite intrusion, to the west of the Champlain Thrust. The formation of the Iapetus Ocean (proto-Atlantic) during the Late Proterozoic was a phase of extension in between the two orogenic episodes. The complex Appalachian orogeny (500 Ma to 230 Ma ago), started during the closing of the Iapetus Ocean and involved the accretion of two island arc terranes to the cratonic continent (Taconic and Acadian orogenies) and a posterior continental collision (Alleghanian orogeny) (Detweiler and Mooney, 2003). The younger Appalachian rocks are mostly metasediments and metavolcanic rocks intruded by granitic elements, formed during the mountain-building episodes (Hughes and Luetgert, 1991).

Both heat flow and earthquake depths indicate that the crust is thicker in the Grenville Province (Eaton *et al.*, 2006). Heat-flow studies indicate that there is a sharp increase of about 15 $\mathrm{mW/m^2}$ when crossing from the Grenville Province to the Appalachian Province (e.g., Mareschal and Jaupart, 2004), and seismicity studies indicate that earthquakes occur at greater depths in the Grenville Province (e.g., Du *et al.*, 2003; Ma and Atkinson, 2006).

Attenuation of seismic waves varies with tectonic setting and is lowest for stable continental regions such as the cratonic eastern North America (Frankel *et al.*, 1990). Within the NEUS, regional attenuation studies (Shi *et al.*, 1996) show that the Grenville Province has a higher crustal average quality factor Q than the Appalachian Province. The differences in attenuation also correlate well with the differences in crustal temperature, as waves are more attenuated when propagating through warmer media. In addition, studies of the regional crustal structure indicate that there is a difference in the propagation velocity of seismic waves between the two regions, which encompass the upper midcrust and lower crust, down to the Moho (e.g., Taylor *et al.*, 1980; Hughes and Luetgert, 1991,1992; Helmberger *et al.*, 1992; Hughes *et al.*, 1993; Musacchio *et al.*, 1997). The higher velocities in the Grenville Province are attributed to compositional differences between the two provinces (e.g., Hughes *et al.*, 1993; Musacchio *et al.*, 1997). In summary, Grenvillian crust is cooler and thicker, and seismic waves propagate faster with less attenuation than in the Appalachian crust.

The NEUS is characterized by low seismic activity, a typical feature of stable continental regions. Seismicity in the NEUS is approximately 10–20 times lower than in active plate boundary regions, such as the southwestern United States. The seismicity distribution in ENA is variable, with very active regions (Charlevoix, Quebec), moderately active regions (Appalachians and St. Lawrence River valley), and almost aseismic regions (Canadian prairies) (Atkinson, 1989). The maximum compressive stress is fairly constant throughout the region. It is near-horizontal and trends to the east–northeast on average (Du *et al.*, 2003). The Au Sable Forks earthquake occurred in a moderately active region, within the Grenville Province and near the boundary with the Appalachian Province. The focal mechanism of the Au Sable Forks earthquake (Fig. 1) is consistent with the general trend of faulting in the region.

Previous Regional Models

Because the low seismic activity of the region and the lack of large earthquakes, models of NEUS crustal structure rely on data from seismic surveys carried out since the 1950s for defining crustal properties (Eaton *et al.*, 2006). In 1988, a large refraction/wide-angle reflection survey that crossed the Appalachian and Grenville Provinces was performed. This Ontario–New York–New England Seismic Refraction Profile provided data for several studies: Hughes and Luetgert (1991) used a two-dimensional inversion technique to determine a seismic P-wave velocity model for the Grenville and Appalachian Provinces, and Hughes *et al.* (1993) further constrained the velocity models with seismic properties from sample rocks collected in the region and measured in the lab; Zhu and Ebel (1994) used a tomographic inversion technique to determine the velocity structures of Northern New England; and Musacchio *et al.* (1997) used the P wave to S wave velocity ratio to determine the crustal composition of the two provinces. These studies all showed a lateral velocity and Moho depth gradient, with higher velocities and greater Moho depths in the Grenville Province and slower velocities and shallower Moho depths in the Appalachian Province.

Ground motions from regional moderate earthquakes have also been used for crustal studies; however, previous studies relied on sparse seismic networks and limited data. Somerville (1989) derived a 1D velocity model for the northern Appalachian Province using aftershocks of the 1982 M 5.6 New Brunswick earthquake. Zhao and Helmberger (1991) used the recording at station HRV of the 1988 M 5.9 Saguenay earthquake paired with broadband forward modeling to develop a 1D model of this path. Helmberger *et al.* (1992) used long period records of three NEUS moderate-sized earthquakes and the one broadband record of the Saguenay earthquake to understand differences in crustal velocities on either side of the Appalachian thrust belt, by comparing simple one-layer crustal models with the Zhao and Helmberger (1991) 1D velocity model for the Appalachian Province. Saikia (1994) refined the Appalachian 1D velocity model of Zhao and Helmberger (1991), by forward modeling broadband waveforms of the Saguenay earthquake recorded at station HRV and at eight short-period stations from the ECTN. Somerville *et al.* (2001) used a simple crustal model based on the midcontinent crustal structure to define a prediction equation for the central and eastern United States. Figure 2 summarizes some of these crustal-velocity models of the two provinces.

Data: The 2002 Au Sable Forks, New York, Earthquake Sequence

A M 5.0 earthquake occurred on 20 April 2002 near the town of Au Sable Forks, New York, at a depth of ~11 km (Seeber *et al.*, 2002). This intraplate earthquake had a thrust mechanism with no surface rupture. It damaged roads, bridges, chimneys, and water lines and was felt as far as Maine, Ohio, Michigan, Ontario, and Maryland (USGS, 2002). It is the largest earthquake to be recorded by the six regional broadband networks installed within the last decade and the best recorded event in the NEUS. It was recorded at more than 50 stations, at distances between 70 km and 2000 km. Figure 1 shows the available broadband locations as well as the boundary between the Appalachian and Grenville Provinces. We limit our analysis to epicentral distances smaller than 400 km (significant for seismic hazard assessment), where the waveforms are simpler and have good signal to noise ratios. We analyze data recorded at 16 stations from four broadband networks: three stations (GAC, MNT, and KGNO) from the Canadian National Seismograph Network (CNSN); three stations (BINY, LBNH, and HRV) from the United States National Seismograph Network (USNSN); three stations (NCB, ACCN, and CONY; seismograms at station LSCT were cut) from the Lamont–Doherty Cooperative Seismographic Network (LCSN); and seven stations (BCX, BRY, HNH, QUA2, WES, WVL, and YLE; seismograms at stations VT1 and FFD were clipped) from the New England Seismic Network (NESN). We integrate

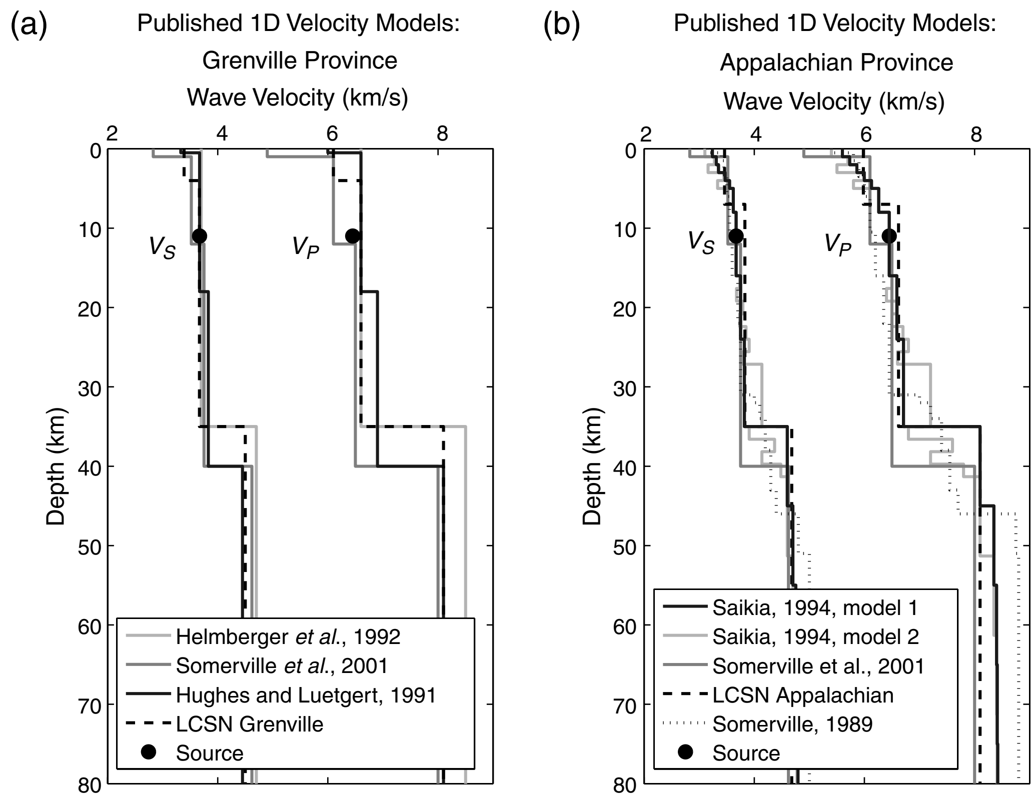

Figure 2. Published 1D velocity crustal models used in this study. (a) *P*-wave and *S*-wave velocity profiles for the Grenville Province (faster velocities). (b) *P*-wave and *S*-wave velocity profile for the Appalachian Province (slower velocities). The mainshock depth is indicated by a black circle.

the velocity records to displacement, remove the instrument response, and high pass-band-filter above 0.01 Hz.

The Au Sable Forks earthquake had nine aftershocks with local magnitudes between 3.7 and 2.2, large enough to be recorded by the broadband networks. All broadband data are available through the Internet except the NESN data, which are available upon request from the Weston Observatory in Weston, Massachusetts. The Global Seismic Network/Incorporated Research Institutions for Seismology (IRIS), USNSN, LCSN, and CNSN broadband stations use a sampling rate of 40 samples/s, and the NESN stations use a sampling rate of 100 samples/s.

Regional Wave Propagation

We investigate wave propagation by forward modeling the broadband records of the earthquake. We generate synthetic seismograms and try to match the observed seismograms with absolute timing and amplitude. To generate synthetic seismograms, we require medium and source information. Source information consists of fault mechanism, earthquake depth, seismic moment, and source time function. We use the empirical Green's function method (EGF; e.g., Hartzell, 1978; Abercrombie and Rice, 2005) to place constraints on the source time function. To obtain the medium information, which is a combination of wave propagation and a crustal-velocity model, we use a frequency–wavenumber code (e.g., Saikia, 1994) that computes Green's functions for a layered 1D crustal structure. We model the Appalachian and Grenville Province records using 1D velocity crustal models characteristic of each province, as discussed earlier. Given the fault mechanism and the earthquake depth, it generates preliminary synthetic seismograms. We obtain the final synthetics by convolving the preliminary synthetics with the source time function.

Source Model

To model the earthquake wave propagation from source to site, we need a source model to account for the orientation and finiteness of the earthquake source. We adopt the earthquake source parameters (seismic moment $= 4.47 \times 10^{16}$ N m and depth $= 11$ km) estimated by Seeber *et al.* (2002) with a moment-tensor inversion with regional broadband recordings of the Au Sable Forks earthquake. Seeber *et al.* (2002) found a small westward bias in the earthquake epicenter locations estimated from the regional records when compared with the epicentral locations estimated from records of a temporary local network deployed two days after the mainshock. They attribute the location bias to the velocity differences between the two provinces, which is not accounted for by the location procedure that used a single crustal-velocity model. To obtain more precise locations, Kim *et al.* (2002) relocated the mainshock and early aftershocks using a master event technique. We adopt the epicenter location (44.509° N, 73.675° W) and event origin time (10:50:47.1, UTC) estimated by Kim *et al.* (2002). The earthquake source depth of 11 km was confirmed with the relocation procedure and is consistent with the aftershock hypocenter distribution (Seeber *et al.*, 2002) and with the regional seismicity depth (Ma and Atkinson, 2006). Seeber *et al.* (2002) determined a thrust-fault mechanism, but the fault plane was not clearly illuminated by the aftershock distribution. The relocation procedure (Kim *et al.*, 2002) confirmed the complex conjugate structure of the earthquake sequence. Kim *et al.* (2002) and Kim and Abercrombie (2006) prefer the nodal plane solution 1 (strike 188°, rake 96°, and dip 47°) of Seeber *et al.* (2002), which we adopt to generate the synthetic ground motions. Although the moment-tensor inversion method is applied to low-frequency data (0.03–0.1 Hz) and uses a simple three-layer 1D velocity model, the estimated source parameters (depth, strike, rake, etc) are fairly insensitive and within the uncertainties (10%) of reasonable variations in the velocity model (Sipkin 1982; Dreger and Helmberger, 1993). Figure 1 shows the mainshock location and focal mechanism relative to the available broadband stations.

Seeber *et al.* (2002) estimated a source time function with 0.8 s duration. This source pulse was, however, calculated from low frequency records used in the moment-tensor inversion (0.03–0.1 Hz). We use the EGF approach (e.g., Hartzell, 1978; Abercrombie and Rice, 2005) to estimate the source time function from records containing higher frequencies (up to 18 Hz). The EGF method uses a smaller (one to two orders of magnitude) colocated earthquake as a transfer function representative of the wave path. A suitable EGF earthquake should have the same focal mechanism as the large earthquake from which it is deconvolved. Colocated earthquakes with the same focal mechanisms will have similar recorded waveforms at the same station. The main difference between the waveforms will be the pulse shapes and widths, which depend on the rupture history and duration of the earthquakes. Nine aftershocks of the Au Sable Forks earthquake ($>M2$) have sufficient signal above noise for EGF analysis and are located fairly close to the mainshock. Studies using the EGF approach rarely consider the effects of differences in location, focal mechanism, and waveform shape on the results (e.g., Viegas *et al.*, 2010). Kim *et al.* (2002) calculated the moment tensor for the largest aftershock (M 3.7) of the sequence and found it to have a thrust-fault mechanism, similar to the mainshock but with its P axis rotated by 90°, making it a less suitable EGF earthquake. The remaining eight largest aftershocks of the sequence had waveform shapes similar to the largest aftershock, indicating similar focal mechanisms. We use the largest aftershock of the sequence, where the signal to noise ratio is best, as the EGF earthquake. The waveforms are similar enough for us to obtain source pulses at seven stations with an average duration of 1 s, consistent with that obtained in the moment-tensor inversion. This implies that both the amplitude and phase of the frequency spectra are very similar. We obtain single triangular pulses at 60% of the stations and double triangular pulses at the remaining 40%. If the radiation patterns of the two earthquakes were more similar, we could interpret the variation as originating from the source and use it to determine directivity and, potentially, the fault plane. Given the known differences, it is possible that some of the azimuthally varying complexity is an artifact of different amplitudes of reflected and refracted phases between events. Hence we prefer not to trust any complexity or azimuthal variation between the pulses but believe that the average shape provides a useful constraint on the source process. We experiment with both single-pulse and double-pulse shapes in the wave propagation models. We find that the single pulse fits the waveform best, implying that the source time function complexity observed at some stations results from uncertainties in the EGF deconvolution and does not reflect source complexity. In this study, we adopt a single triangular 1 s pulse as the source time function. Because of the limitations on the pulse shape, we cannot resolve source directivity, which would help to identify the focal plane.

We estimate a stress drop of 30 MPa from the source duration, following Eshelby (1957) and Madariaga (1976), consistent with stress-drop values obtained for the Au Sable Forks earthquake sequence (Viegas *et al.*, 2010). This high stress-drop value substantiates the idea that intraplate earthquakes have higher stress drops than those at plate boundaries (Kanamori and Anderson, 1975).

Validation of 1D Crustal-Velocity Models

Using published 1D crustal-velocity models, we investigate wave propagation in the two provinces. We test five Appalachian and four Grenvillian regional crustal models. For the Appalachian Province, we test the regional crustal model adopted by the LCSN network for routine event location in this region (Seeber *et al.*, 2002), the two crustal models from Saikia (1994), the Somerville (1989) model, and the Somerville *et al.* (2001) midcontinent crustal model. For the models without defined attenuation and density values (Seeber *et al.*, 2002 and Somerville 1989), we adopt the values obtained by Saikia (1994). Figure 2 illustrates the 1D velocity profile of these models for both P and S waves. The LCSN and Somerville *et al.* (2001) models consist of a two-layered and three-layered crust, respectively. The main differences between these two models are the existence of a thin low-velocity upper layer and a deeper Moho in the Somerville *et al.* (2001) model. Both the Saikia (1994) and Somerville (1989) models consist of several layers. The main differences between the three models may be described by: an upper-crust gradient (model 1, Saikia, 1994); alternating thin high-velocity and low-velocity layers (model 2, Saikia, 1994); and a deep Moho layer at 45 km depth (Somerville, 1989).

For the Grenville Province, we test the regional crustal model adopted by the LCSN network for routine event location in this region (Du *et al.*, 2003), the Hughes and Luetgert (1991) model, the Helmberger *et al.* (1992) model, and the Somerville *et al.* (2001) midcontinent crustal model. All but the Somerville *et al.* (2001) models have no indication of attenuation and density values. We adopt the values obtained by Saikia (1994) for the Appalachian Province and slightly decrease the attenuation for the Grenville Province, which is older and cooler (Shi *et al.*, 1996). We create a 1D model from the Hughes and Luetgert (1991) cross-sectional figure, with indications of *P*-wave velocities only. We built a 1D velocity profile with average depths based on the cross section. We constructed the *S*-wave profile using an average *P*-wave to *S*-wave velocity ratio (V_P/V_S) of 1.80, which is consistent with the Musacchio *et al.* (1997) study of the crustal composition in the Grenville Province and with the Eaton *et al.* (2006) study of V_P/V_S variations in the Grenville orogen. We also use $V_P/V_S = 1.8$ to estimate *S*-wave velocities for the LCSN model for the Grenville Province. All Grenville models vary between one (Helmberger *et al.*, 1992), two (LCSN), and three (Hughes and Luetgert, 1991; Somerville *et al.*, 2001) layers. The main differences between the four models can be described by: various upper-layer thickness and velocity configurations; two possible Moho-layer depths of 35 km or 40 km; and a wide variability of the *P*-wave velocities.

Between the two provinces, Grenville models show consistently higher crustal velocities, particularly at the shallower layers. The depth of the Moho layer shows the same range of variability within each province, without a visible trend. In the particular case of the LCSN models for the two provinces, the surface layer is the main feature that distinguishes them, being thicker and slower for the Appalachian model.

Models of the Appalachian Province use an average $V_P/V_S = 1.73$, while Grenville models use an average $V_P/V_S = 1.80$. The different ratios reveal an assumed difference in the crustal composition of the two provinces. When comparing the velocity profiles of both regions, we observe that the higher ratio is a result of a higher *P*-wave velocity, whereas the *S*-wave velocities are approximately the same in the two provinces. This indicates that the differences in the V_P/V_S ratio come from compositional differences, which increase V_P (Musacchio *et al.*, 1997), and not from a higher water content in the Grenville Province, which would lower V_S. A Grenvillian crust with a more mafic (gabbroic) composition than the Appalachian crust, which has an intermediate to basic composition, seems to be the likely basis for differences in V_P/V_S ratios (Musacchio *et al.*, 1997). The more mafic composition of the Grenville Province is consistent with the composition of an eroded old orogeny (Eaton *et al.*, 2006).

We generate synthetics for each of the 16 earthquake-station paths using the described models and analyze how well they fit the data quantitatively (using two goodness of fit statistics) and qualitatively. We then select one model for each province that performs the best at the most stations, thereby validating the 1D model across several paths. All waveforms are band-pass—filtered between 0.03 Hz and 1 Hz unless otherwise specified.

We use quantitative misfit measurements of both variance and cross correlation to evaluate model-generated synthetics relative to the observed seismograms. We use the percentage variance reduction (VR)

$$\mathrm{VR} = [1 - (\Sigma(\text{synthetics} - \text{data})^2/\Sigma(\text{data})^2)] \times 100$$

(e.g., Chi *et al.*, 2001) over a time window that contains the whole waveform. The VR is a suitable misfit measurement because it accounts for both amplitude and waveform similarity. A VR of 100% indicates a perfect agreement between data and synthetics (Baig *et al.*, 2003). When there is a time lag between data and synthetics, large enough to juxtapose a trough with a crest, negative VR values are obtained. To assess waveform shape and allow for time shifts that may result from bias in the velocity structure, we also cross correlate the recorded with the synthetic seismograms. We consider the maximum correlation coefficient and corresponding time lag over the same time series used to calculate the VR. The cross-correlation results proved particularly useful to identify the observed crustal anisotropy (see the Anisotropy section).

The quantitative measurements are most sensitive to misfits in the large amplitude features of the waveforms (surface waves), so we also qualitatively assess the waveforms (1) to ensure good fit to the arrival times, phase polarities, and amplitudes of the smaller amplitude body waves and (2) in terms of how well the synthetics match the most representative seismic phases and amplitudes, which characterize the overall shape of the observed seismogram.

When comparing the synthetics to data for all 10 source-station paths in the Appalachian Province, we found the Saikia (1994) model 1 provided the best fit to the Au Sable Forks earthquake recorded waveforms. Figure 3 shows the synthetic waveforms compared to data for the vertical component (where both *P* and *S* arrivals can be clearly seen) at all 10 stations in the Appalachian Province for the App1 model. Average misfit values for the Saikia (1994) model 1, hereafter called the App1 model, for all three components at the 10 stations give the highest variance reduction at high (<1 Hz) and intermediate (<0.5 Hz) frequencies, as shown in Table 1. The LCSN model, a three-layered model presents the highest average variance-reduction value at low frequencies (<0.1 Hz). As compared to LCSN, the App1 model has a better average correlation coefficient and lower average absolute-time lag at the low frequencies. All models perform well at low frequencies, as indicated by average correlation coefficients larger than 0.80. When comparing all models, the App1 model provides the best fit to the observations in terms of shape and arrival times of the main phases at frequencies less than 0.1 Hz for all the source-station paths. Figure 4a shows the superposition of the three-component

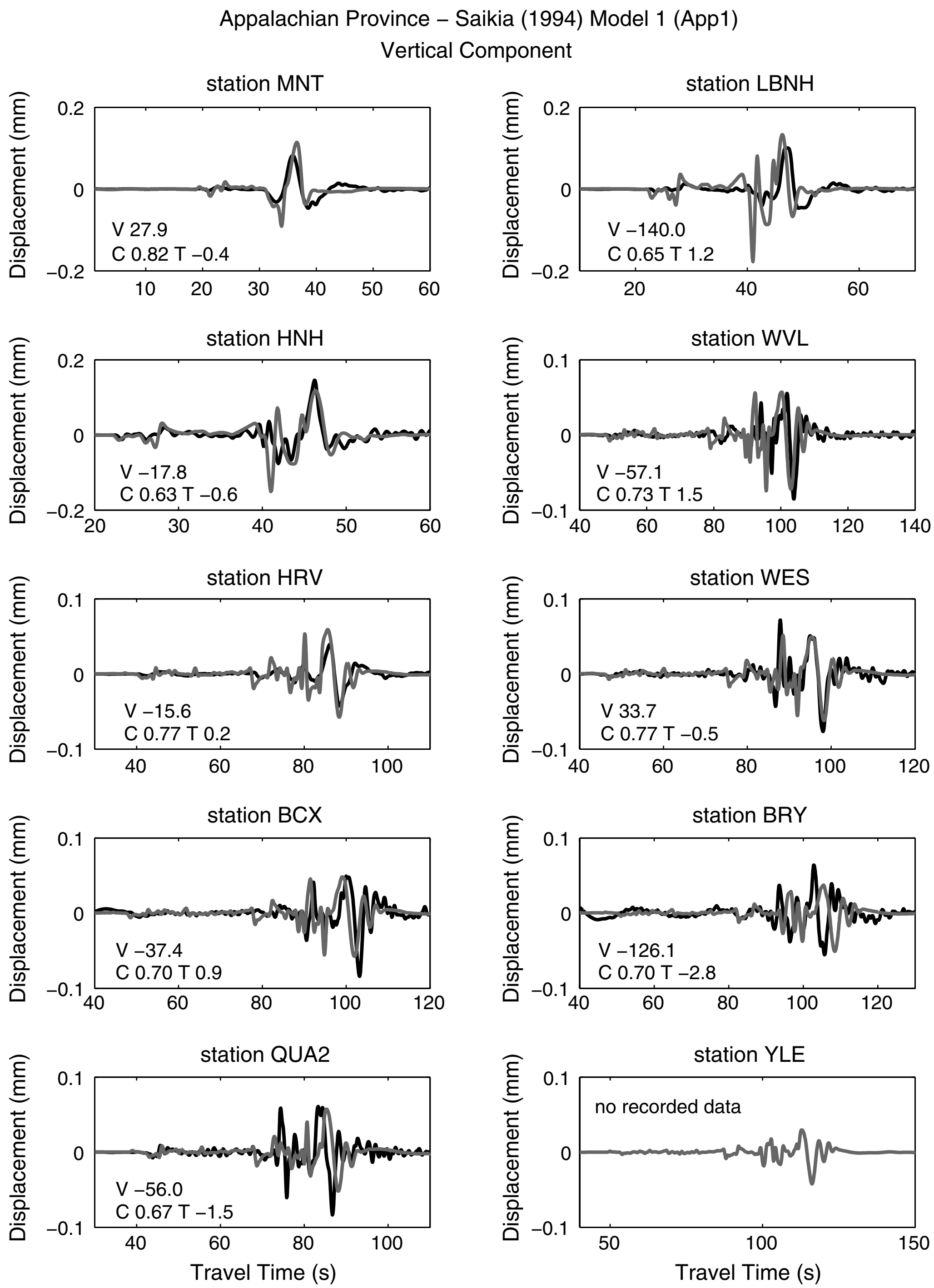

Figure 3. Vertical component of the synthetics generated with the App1 model (gray line) for all source-station paths in the Appalachian Province, with the recorded data (black line). The source is convolved in the synthetics. All seismograms are band-pass-filtered between 0.03 and 1 Hz. V, variance reduction; C, correlation coefficient; and T, time lag in seconds.

recorded waveform and the synthetic waveform generated with the App1 model, low passed below 0.1 Hz, for the source-station LBNH path. We can therefore conclude that the main crustal layers are well identified in this model.

For qualitative comparison, Figure 5 shows all Appalachian models simulated for the source-station WES path. The App1 synthetics are a good fit to the data in both absolute timing and amplitudes of primary phases. The tangential component arrivals are later in the synthetics by 2.9 s, indicating possible anisotropy, but the waveforms have a similar shape translated by a correlation coefficient of 0.80. Saikia (1994) model 2 also fit the radial and vertical components of data well at WES but have slight misfits in timing of primary phases. Saikia (1994) model 2 used alternating high

Table 1
Station Average Misfit Values Obtained for Each Published Model Tested in This Study at Three Passbands*

		Appalachian Province†					Grenville Province‡			
		App1	App2	S89	LCNS	S01	Helm	S01	Gren	LCSN
0.03–1.0 Hz	VR	−45.5	−53.9	−74.7	−69.4	−155.3	−95.3	−248.2	−84.0	−19.4
	C.Coef	0.622	0.562	0.658	0.580	0.625	0.538	0.658	0.619	0.661
	T.Lag (s)	2.04	2.39	1.38	2.01	2.34	2.98	1.55	2.13	1.25
0.03–0.5 Hz	VR	−37.2	−53.5	−75.3	−65.3	−145.2	−74.2	−225.7	−65.8	−14.0
	C.Coef	0.705	0.629	0.725	0.662	0.713	0.606	0.727	0.670	0.710
	T.Lag (s)	1.85	3.06	1.98	2.57	2.92	3.20	1.54	2.45	0.71
0.03–0.1 Hz	VR	−37.3	−54.3	−107.8	−10.5	−152.7	−136.2	−400.5	−137.9	−208.9
	C.Coef	0.817	0.835	0.811	0.801	0.811	0.823	0.831	0.827	0.827
	T.Lag (s)	3.34	3.25	3.63	4.45	4.16	3.09	4.51	3.44	3.46

*Passbands: 0.03–1.0 Hz; 0.03–0.5 Hz; and 0.03–0.1 Hz. VR, variance reduction; C.Coef, correlation coefficient; and T.Lag, absolute time lag.

†App1 and App2 models refer to the Saikia (1994) models 1 and 2, respectively; S89 refers to the Somerville (1989) model; LCSN (Seeber *et al.*, 2002) refers to the Lamont–Doherty Cooperative Seismographic Network model; and S01 refers to the Somerville *et al.* (2001) model.

‡Helm refers to the Helmberger *et al.* (1992) model; S01 refers to the Somerville *et al.* (2001) model; Gren refers to the Hughes and Luetgert (1991) model; and LCSN (Du *et al.*, 2003) refers to the Lamont-Doherty Cooperative Seismographic Network model.

and low thin velocity layers to create complexity at high frequencies in order to better model the short-period recordings at ECTN for the 1988 *M* 5.9 Saguenay earthquake. This high-frequency feature, which slows the surface waves, does not improve the synthetics in our study (<1 Hz) relative to model 1 but may improve the synthetics at higher frequencies. The LCSN model, the Somerville (1989) model, and the Somerville *et al.* (2001) model do not perform as well for the source-station WES path. The *S* and surface-wave phases arrive too soon for the LCSN model, indicating that the model is too fast. For the Somerville (1989) model, these phases arrive too late, indicating that the model is too slow. The *P* and surface-wave phases arrive too late for the Somerville *et al.* (2001) model, indicating that model is also too slow. Both the Somerville (1989) and the Somerville *et al.* (2001) models generate synthetics with high surface-wave amplitudes. Based on the better misfit values and qualitative goodness of fit, we select the App1 model as our starting model for the forward-modeling study of the Appalachian Province.

After comparing the goodness of fit at the six stations in the Grenville Province, we find that the LCSN model quantitatively fits the data better than the other models. Average values for all three components at the six stations give higher variance reduction and correlation coefficient values and smaller time lags for the LCSN model, as shown in Table 1. Figure 6 shows the Grenville models simulated for the GAC station path. No model provides an excellent fit to the data. The timing of initial *P* arrivals is early for models LCSN, Hughes and Luetgert (1991), and Helmberger *et al.* (1992), although slightly better for the LCSN model and late for the Somerville *et al* (2001) model. The vertical motion is well modeled by the LCSN model for the first three *S* phases. In general, the timing of the *S* wave is modeled well on all components for all models except for the Helmberger *et al.* (1992) model, which is too fast. The Hughes and Luetgert (1991) model fits the tangential motion better. The timing of the surface wave arrivals is in good agreement with the data for the radial and vertical components of the LCSN model, too early for the Helmberger *et al.* (1992) and Hughes and Luetgert (1991) models, and too late for the Somerville *et al.* (2001) model. The later phases of the seismograms are not modeled well by the synthetics, indicating that the observed ground motions have more complexity in the late arrivals. The Somerville *et al.* (2001) model is the exception in generating the later phases, and we note that the model has a sharp velocity contrast between the two upper layers.

Although the LCSN model performs better on average in modeling the ground motion for the six source-station paths, the Hughes and Luetgert (1991) model, the second-best model at the higher and intermediate frequencies (<1 Hz and <0.5 Hz, respectively), performs better at frequencies below 0.1 Hz (Table 1). This indicates that the average crustal structure, sampled by the long-period waves, is best represented by the Hughes and Luetgert (1991) model. Figure 4b illustrates the good fit between model synthetics and data obtained for low frequencies with the Hughes and Luetgert (1991) model at station CONY. The layering of this model is more consistent with the crustal structured observed in seismic studies of the region (e.g., Hughes and Luetgert, 1991, 1992; Hughes *et al.*, 1993; Eaton *et al.*, 2006) than is the LCSN model, particularly the deeper Moho depth of 40 km instead of the 35 km of the LCSN model. Therefore, we select the Hughes and Luetgert (1991) model, hereafter called the Gren model, as our starting model for the forward-modeling study of the Grenville Province. Figure 7 compares synthetics (vertical motion) calculated with the Hughes and Luetgert (1991) model to data for the six source-station paths in the Grenville Province. The Hughes and Luetgert (1991) model captures many of the primary phases of the data, but many of the synthetic arrivals are early as compared to the data.

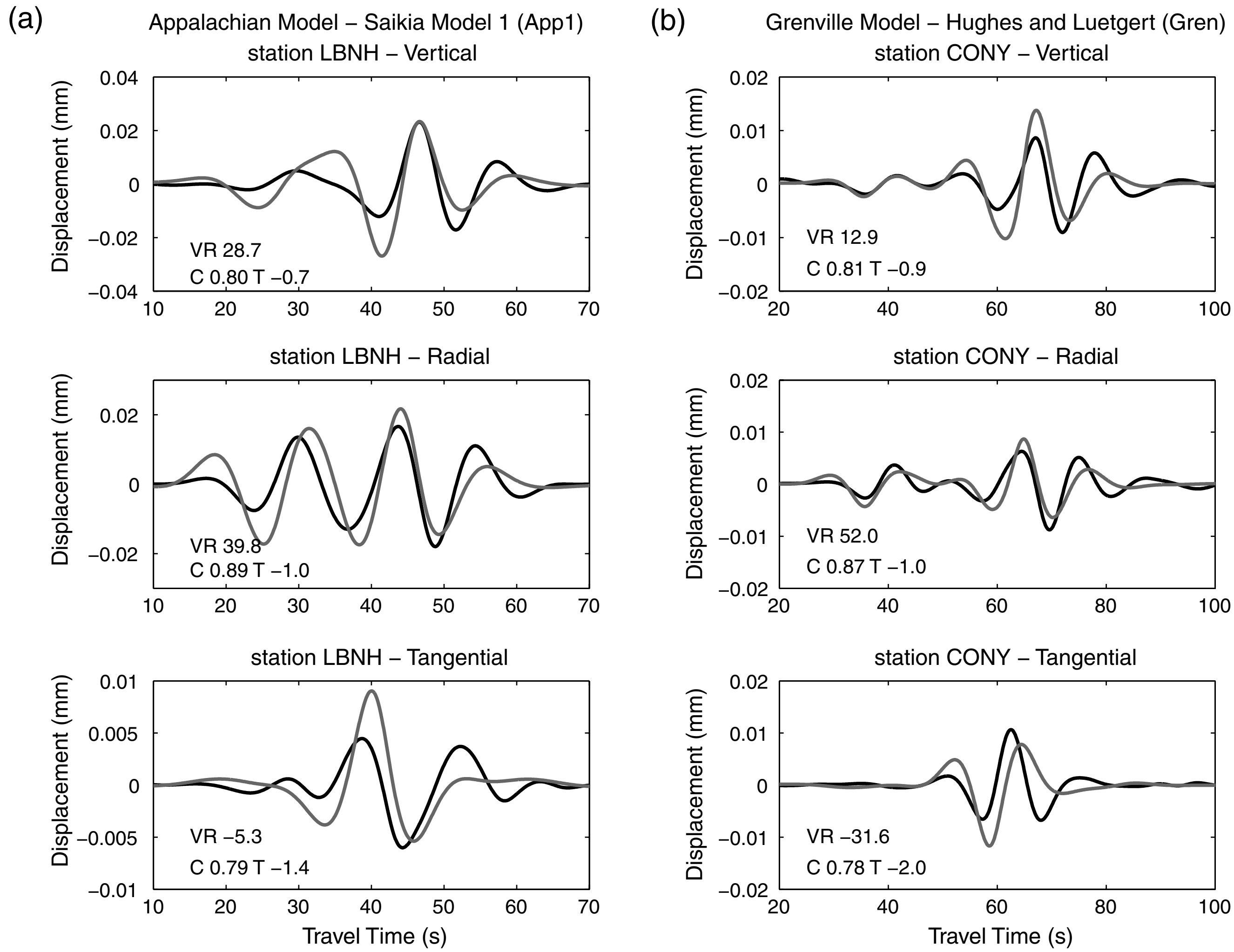

Figure 4. Comparison of the synthetic waveforms (gray line) with the recorded waveforms (black line) low passed below 0.1 Hz. (a) Synthetics generated with the App1 model for the source-station LBNH (Lisbon, New Hampshire) path. (b) Synthetics generated using the Gren model for the source-station CONY (Cobleskill, New York) path. VR, variance reduction; C, correlation coefficient; and T, time lag in seconds.

Forward Modeling

Model Sensitivity Tests

The first step in our forward-modeling approach is to perform two types of sensitivity tests to the selected 1D starting models for each province. Based on the results of these tests, we can improve the models to better fit the data. In the first sensitivity test, we remove the layers one by one and identify the contribution of each layer to the composite synthetic waveform. In the second sensitivity test, we vary the crustal model parameters (such as layer velocity or thickness) by small percentages and determine the overall response of the waveform to these perturbations.

Removing the model layers provides information on which boundaries or reflectors have a pronounced effect on the waveform shape. Figure 8 shows an example of the procedure applied to App1. The instrument-corrected displacement seismogram recorded at station LBNH is displayed at the bottom, with the preliminary synthetics displayed in the lines above it. We use the preliminary synthetics (without the source time function convolved) to be able to identify the low-amplitude wave arrivals. Once we convolve the source time function to the preliminary synthetics, the waveform is smoothed and the low amplitude phases masked, as the convolution process acts like a filter. The number of layers removed increases from bottom to top. A8 is the starting 1D model, A9 the model without the Moho layer, and so forth. Circles identify the wave arrivals suppressed when a layer is removed. In Figure 8, the circles over the A8 synthetic indicate the multiple reflected waves suppressed by removing the Moho layer. The right side of the figure shows the *P*-wave velocity profile and how the gradual removal of layers is processed, starting from the deepest layers.

The waveforms were not particularly sensitive to the slow increase in mantle velocity with depth, as expected for ray paths within epicentral distances less than 400 km, which do not penetrate deeply into the mantle. The upper layers contribute largely to the overall shape of the last part

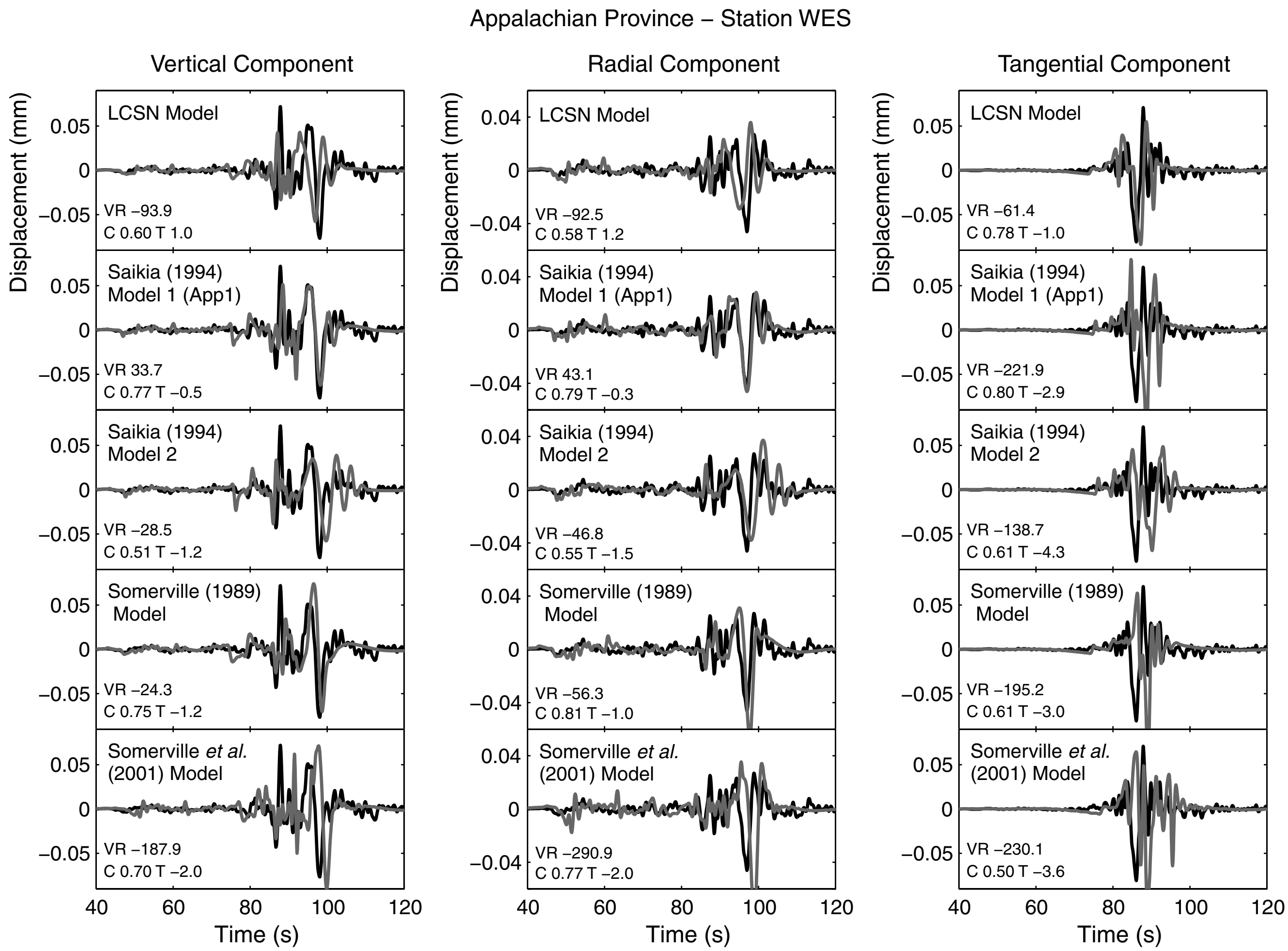

Figure 5. Comparison of the recorded data (black line) with synthetic displacement seismograms (gray) generated for the path toward station WES (Weston, Massachusetts) using five published crustal models for the Appalachian Province. The source is convolved in the synthetics. Seismograms are band-pass-filtered between 0.03 and 1 Hz. VR, variance reduction; C, correlation coefficient; and T, time lag in seconds.

of the seismogram, as regional trapped waves and surface waves are the main constituent of the later part of the seismogram, as seen in A14–A18. The interface at the base of the earthquake source layer contributes to the amplitude of the initial *P* as well as the early *pS* arrivals (A11–A12). The Moho reflector contributes with phases throughout the entire seismogram, as *P* and *S* waves reflect from this boundary.

Changing the properties of one or several layers, such as velocity or thickness, tells us how the full waveform responds to these changes; that is, how the wave arrivals change relative to each other as a result of these perturbations. Our sensitivity analysis included a series of models perturbing the Moho depth, the intermediate layer velocities and thicknesses, and the upper-layer structure (<5 km depth; varying number of layers, as well as velocities and thicknesses of layers).

Figure 9 shows waveform variation resulting from changes in the upper crust model for the Grenville Province model. The sensitivity analysis of the upper layers indicates that we can enhance late arrivals using either a gradient or a sharp velocity contrast between the two upper layers with a thick surface layer (thicker than 3 km and 2 km for the Appalachian and Grenville Provinces, respectively). Based on this series of sensitivity tests combined with multistation analysis, we identify the upper layers as one of the primary foci of our model refinement.

Appalachian Province

Results of the sensitivity tests over multiple source-station paths through the Appalachian Province show that the overall fits of the App1 model to the data were not improved by changes of velocities and thicknesses of the intermediate crustal layers. The sensitivity test results also show that the contribution of the mantle gradient for the overall waveform is minimal at the site-to-station distances in this study and can be disregarded. The App1 model is a detailed 1D model, including a velocity gradient in the first 5 km above the source layer that accounts for near surface effects observed at station HRV (Saikia, 1994). Beneath other stations, the upper crust structure may be different. The

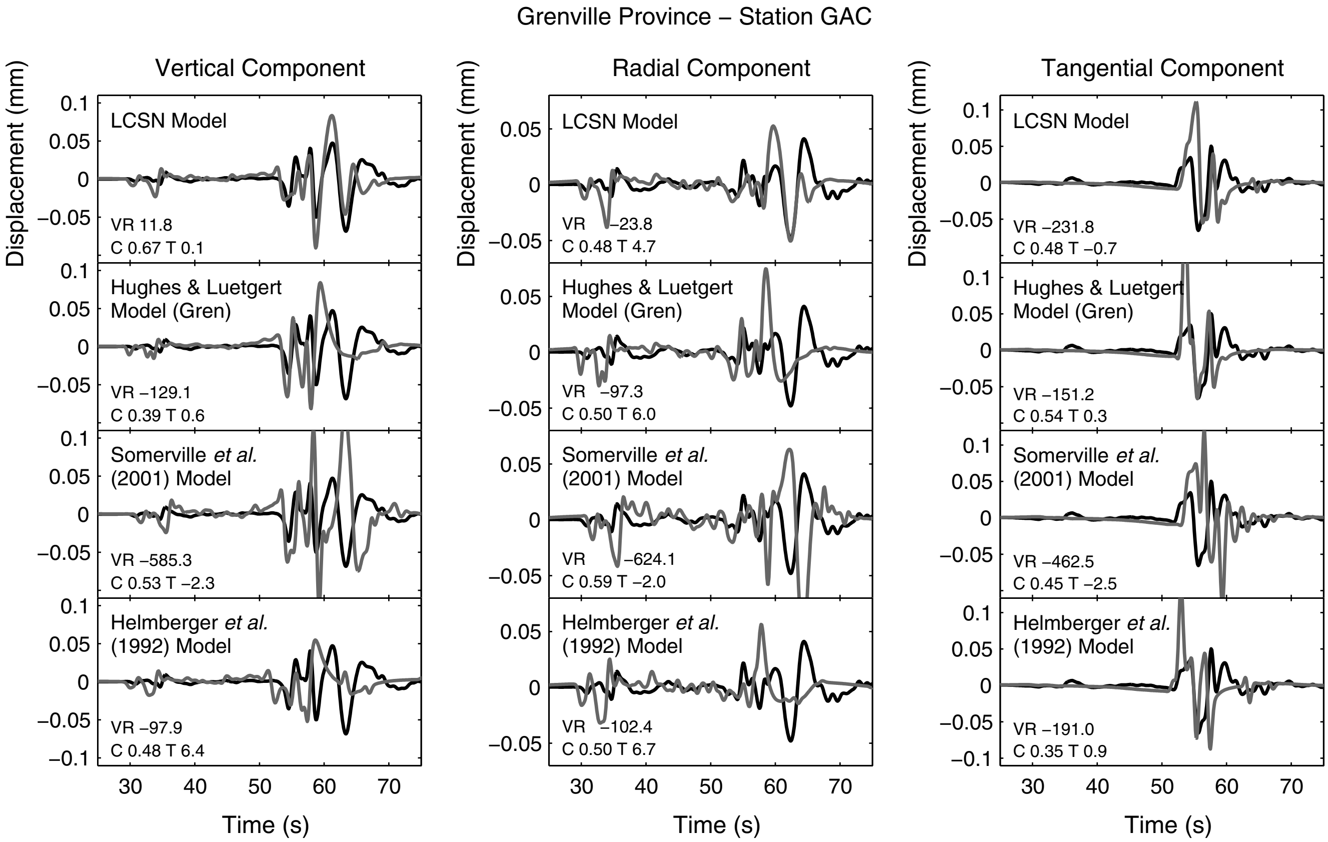

Figure 6. Comparison of the recorded data (black line) with the synthetic displacement seismograms (gray) generated for the path toward station GAC (Glen Almond, Quebec, Canada) using four published crustal models for the Grenville Province. The source is convolved in the synthetics. Seismograms are band-pass-filtered between 0.03 and 1 Hz. VR, variance reduction; C, correlation coefficient; and T, time lag in seconds.

sensitivity tests show that the waveforms are sensitive to the upper crust structure and that perturbations to this structure could improve the waveform fits. We develop several combinations of upper crust layers, maintaining the intermediate and lower-crust profile. We try one to three surface layers, with different thicknesses and velocity contrasts. We expect the results to differ for each source-station path. However, the original surface layers in App1 and one other model with a single 3 km deep surface layer (model h5) provide the best fits for all of the paths in the Appalachian Province. In Figure 10, we graphically depict the 1D velocity profile of our new model h5 along with the initial App1-model profile. An example of the improved fit obtained with model h5 is shown in Figure 11 for the source-station QUA2 path, where the superposition of the recorded and synthetic waveforms is shown for both the App1 and h5 models. The variance reduction, averaged over the three components for this station, improved from −78.8 to −14.5, the correlation coefficient from 0.63 to 0.67, and the corresponding time lag from 2.0 to 0.5 s. Model h5 improves the fits for half (i.e., five) of the source-station paths we model in the Appalachian Province (Table 2). However, when considering the performance of the two models over the 10 paths, the App1 model presents lower average misfit values (Table 2).

Grenville Province

The initial Gren model for the Grenville Province was too fast in terms of P and surface wave arrivals, for all of the six source-station paths (see Fig. 6). Based on the sensitivity test results, we reduce the P-wave velocities at all crustal layers. The average decrease in P-wave velocity is around 2%. With the reduction of P-wave velocities, the model V_P/V_S ratio is reduced to an average value of 1.76, which is higher than the App1 model ratio of 1.73 and consistent with reported values for the region (e.g., Eaton *et al.*, 2006). Sensitivity results also show that the fits are improved when the Moho depth is increased, with best fits achieved for a Moho depth of 42 km; this is consistent with regional crustal studies (e.g., Li *et al.*, 2003). For the surface-layer analyses, we follow the same procedure as for the Appalachian Province. The Gren model has only a very thin (0.5 km) surface layer. We generate 4 new models with the upper-layer thickness increased to 2 km and 3 km and with one and two extra layers introduced between the surface and the source layer (source at 11 km depth) (see example in Fig. 9). Best fits for individual paths based on misfit values vary over the four models, which is expected if we consider the existence of crustal heterogeneity and of local site effects. Model gn33 presents the lowest average misfit

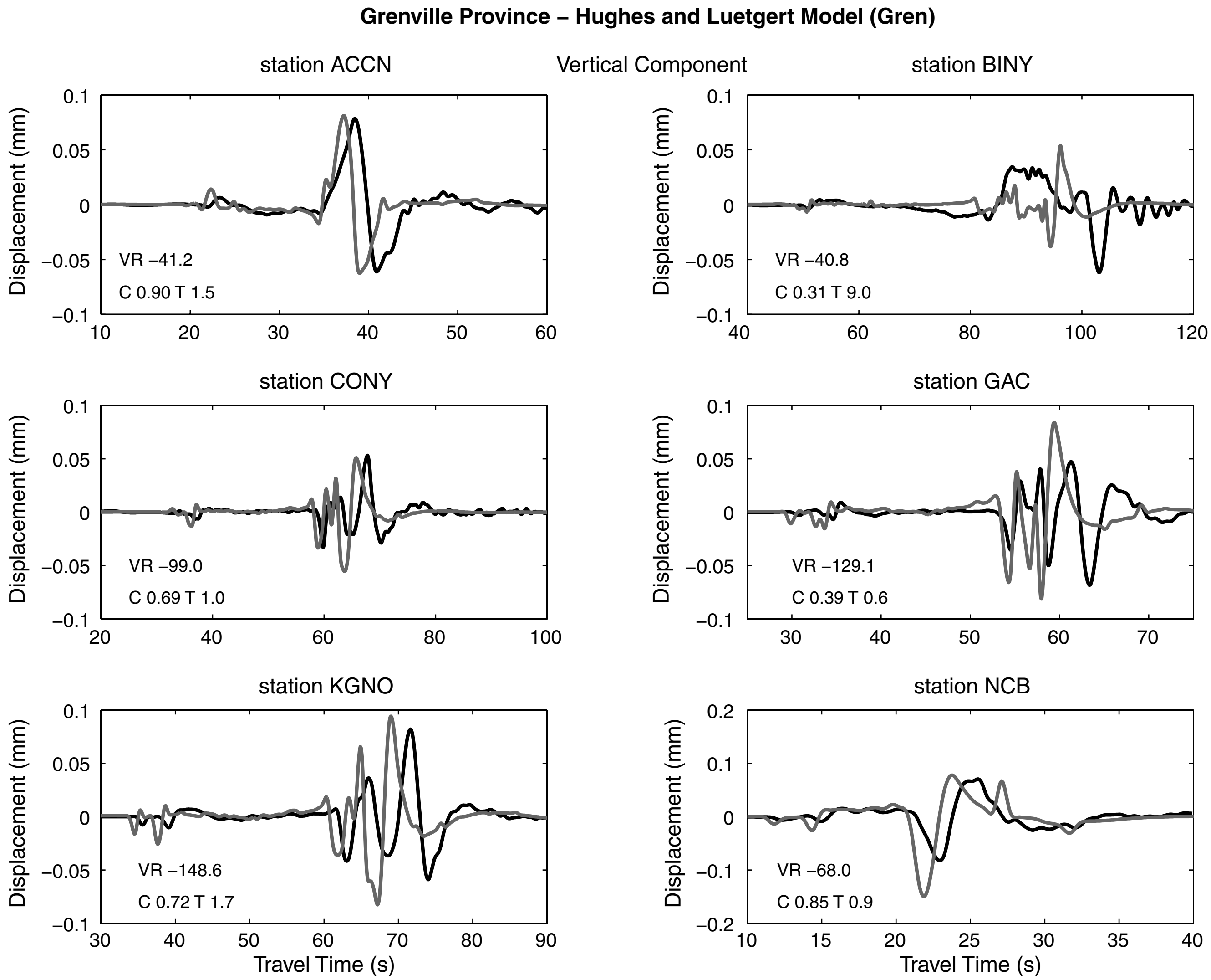

Figure 7. Comparison of the recorded data (black line) with the vertical component of the synthetics generated for all source-station paths in the Grenville Province using the Gren model (gray line). The source is convolved in the synthetics. All seismograms are band-pass-filtered between 0.03 and 1 Hz. VR, variance reduction; C, correlation coefficient; and T, time lag in seconds.

values when considering all six source-station paths. The velocity profile of model gn33 has a three-layer surface gradient, with strong velocity contrasts. An example of the improved fit is shown in Figure 12 for the source-station GAC path, where the sharp contrast of the surface layer results in an increase of the late phases that better imitate the recorded waveform. As shown in Figure 12, the synthetics generated for gn33 have good timing of both *P* and *S* phases. The amplitudes are slightly high, but the phasing is good. The fit of the tangential motion is, however, not improved. The variance reduction, averaged over the three components for this station, improved from −377.7 to −259.1, the correlation coefficient from 0.48 to 0.62, and the corresponding absolute time lag from 2.3 to 0.6 s. Model gn33 improves the fits for all of the six source-station paths we model in the Grenville Province (Table 3). In Figure 10 we graphically depict the 1D velocity profile of model gn33.

From the forward modeling, we find three velocity models (App1, h5, and gn33) that we recommend for the two provinces. Table 2 indicates the preferred model for each source-station path in the Appalachian Province. Model gn33 is preferred for all the paths in the Grenville Province (Table 3). Figure 13a,b,c shows the map with the locations of the stations used in this study, and the recorded and synthetic waveforms computed with the preferred models, for the radial, vertical, and tangential components, respectively. Seismograms are filtered between 0.03 and 1 Hz. To model the ground motions recorded at stations MNT, YLE, and ACCN, which are along the boundary between the two provinces, we use the models of both provinces and choose the one that better fits the data at each station. Because the ray paths that reach these stations may be complex due to the vicinity of the Grenvillian Ramp and associated structures, we do not expect very good fits, and a 2D or 3D velocity

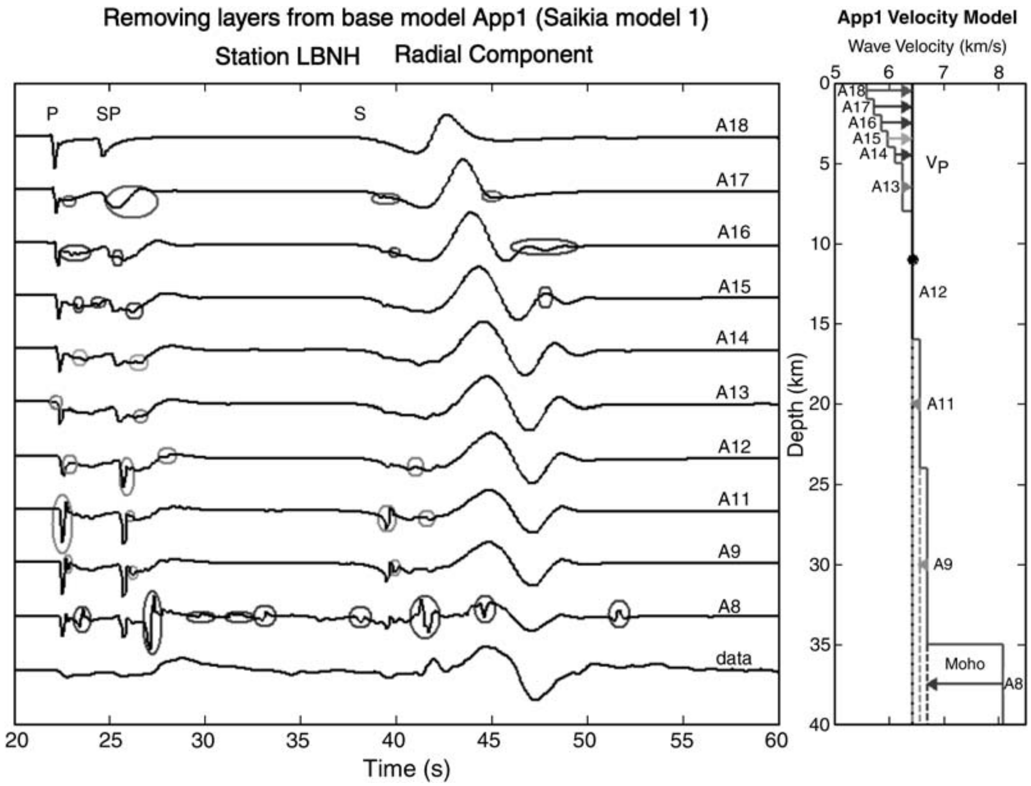

Figure 8. Removing layers. Right side: Saikia (1994) *P*-wave velocity profile (gray) and intermediate profiles as layers are gradually removed, starting with the Moho layer and ending with the surface layers. Left side: radial component of the instrument-corrected displacement seismogram recorded at station LBNH (top line) and preliminary synthetic seismograms generated with the intermediate profiles for station LBNH. Circles indicate suppressed arrivals.

model may be appropriate for these source-station paths. Even so, we obtain reasonable results for MNT (model h5), for ACCN (model gn33), and for YLE (App1 model), especially in the radial and tangential components.

When comparing the crustal velocity profiles of the two provinces, we find an average increase of *P*-wave and *S*-wave velocity of ~2% for the Grenville Province, which translates into an average increase of 0.1 km/s for *P* waves and of 0.05 km/s for *S* waves. The velocity differences between the two provinces are slightly lower than the ones estimated by Levin *et al.* (1995) for the upper crust (0.3 km/s for *P* and 0.1 km/s for *S* waves). However, Levin *et al.* (1995) sampled Grenvillian paths within the , which has higher seismic velocities than the adjacent terranes to the northwest (central metasedimentary belt) and south (e.g., Hughes and Luetgert, 1991, 1992; Musacchio *et al.*, 1997), sampled by our study (see Fig. 1).

Wave-Field Complexity

In our forward-modeling approach, we derived one model for each province that best fits, on average, the three components of ground motion for all the available source-station paths. These models reflect the average crustal structure over a broad region covered by multiple paths, and a few inconsistencies were observed for individual paths between the recorded and the modeled ground motions. The tangential data for all three source-station paths along the Appalachian–Grenvillian boundary (MNT, YLE, and ACCN) are significantly more complex than the synthetics with more late arriving energy, as indicated by the low correlation coefficients obtained (Fig. 13c). The waveform complexity may be a function of the complex ray paths through and parallel to the Grenvillian Ramp. Hughes and Luetgert (1991) identify complex structure at the interface of the provinces, which is the likely cause of the complex ground motions recorded at MNT, YLE, and ACCN. Although we expected more complexity in ground motions recorded in the Appalachian Province as a result of the 2D velocity structure related to the Grenvillian Ramp, the radial and vertical synthetics from the App1 model match the waveforms consistently well (with the exception of the HNH radial component). In contrast, the synthetic tangential components at LBNH, WVL, and BCX need more late arriving surface waves. Therefore, this wave-field complexity may be related to local effects rather than the regional boundary. The surface waves are likely a result of near surface velocity structure or more local 2D structures, which could not be captured in the simple 1D layered models that we evaluated (Baise *et al.*, 2003). In the Grenville Province, the gn33 model synthetics

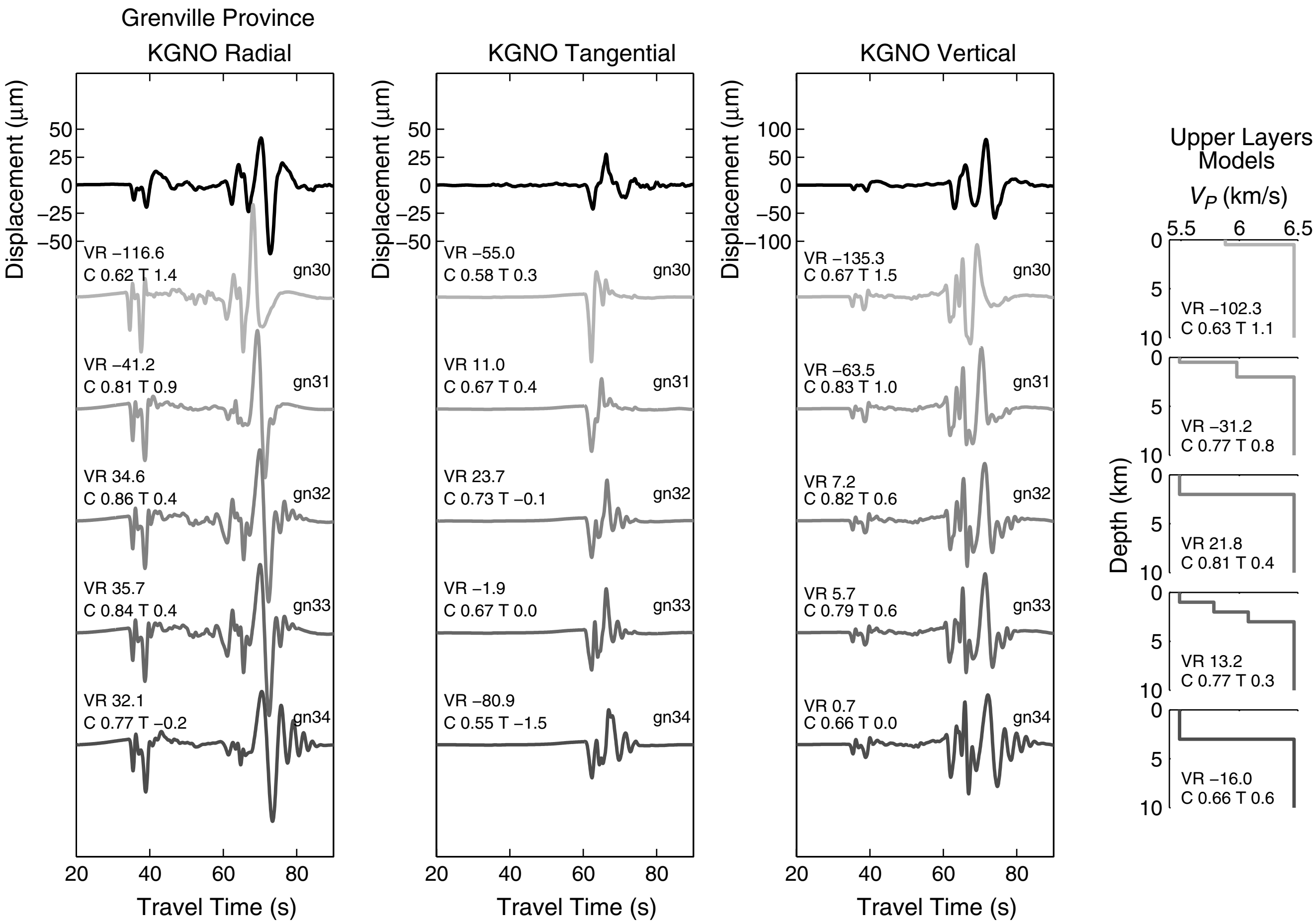

Figure 9. Varying the upper layers. Black seismograms are the recorded data at station KGNO (Kingston, Ontario, Canada). Variations in the upper layers of the 1D velocity model for the Grenville Province are illustrated on the right side of the plot. Synthetics generated with models gn30 to gn34 are plotted in light gray to dark gray, respectively. All three components are shown. Seismograms are band-pass-filtered between 0.03 and 1 Hz, and the source is convolved in the synthetics. The numbers above the synthetics indicate the variance reduction (top line) and the correlation coefficient and time lag (second line). The numbers within the velocity profile indicate the three component average of: VR, variance reduction; C, correlation coefficient; and T, time lag in seconds.

match the radial, vertical, and tangential waveforms consistently well except for the vertical component at BINY and the tangential component at ACCN and GAC (with a VR <-100 or a correlation coefficient <0.40). As discussed, the complexity at ACCN is likely related to its path along the boundary region between the two provinces, while the complexities at BINY and GAC are likely a result of local near-surface structure.

Anisotropy

A systematic delay of the tangential synthetic ground motions relative to the tangential recorded ground motions was observed for several source-station paths in the Appalachian Province. The *S*-wave arrival time on the recorded tangential component at station HRV arrives 2.4 s before the synthetic. This delay is not present on the vertical or radial components, although all three component waveforms are aligned by event-origin time. This implies that *SH* is faster than *SV* and that the fast polarization direction is approximately perpendicular to the northeast–southwest path. The App1 velocity model was developed by Saikia (1994), using only radial and vertical components. Saikia (1994) refined a preexisting model from Zhao and Helmberger (1991), which modeled the three component-broadband waveforms of the 1988 *M* 5.9 Saguenay earthquake recorded at station HRV. Zhao and Helmberger (1991) also observed a time shift for the tangential component of 1.5 s. They proposed epicentral distance uncertainty, anisotropy due to shear-wave splitting, or a regional anomaly as possible mechanisms. We notice that this feature is also observed at nearby stations, with similar azimuth and epicentral distance (see Figs. 2 and 13c).

To quantify the time shift of the tangential component we use the time-lag results from the cross correlation. We determine the total time shift by subtracting the time lag of the radial component from the time lag of the tangential component, thus eliminating any model-induced time delay.

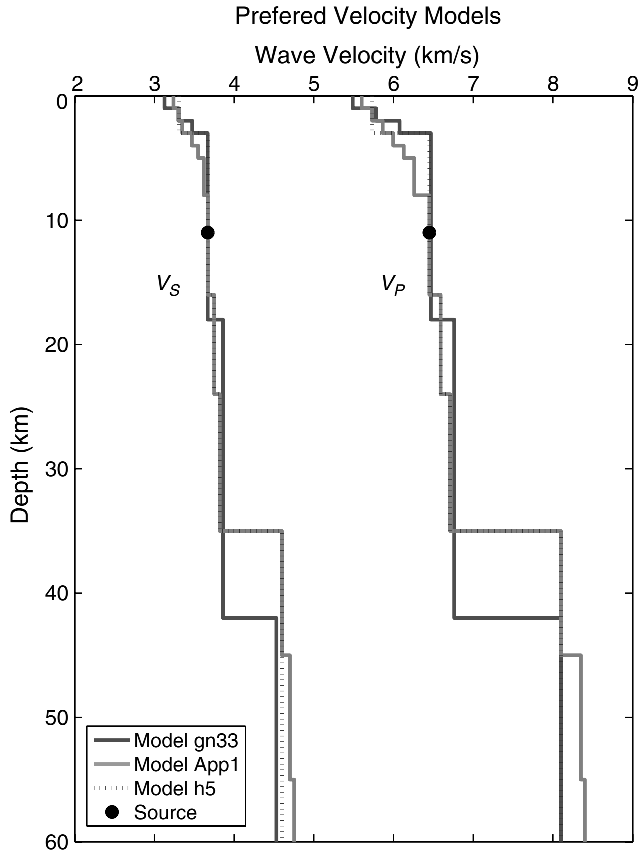

Figure 10. Preferred 1D crustal seismic velocity model for the Grenville Province, gn33 (dark gray line), preferred App1 (light gray line), and alternative h5 (black dashed line) models for the Appalachian Province.

We calculate the total time shift for all paths within the two provinces, in which the tangential correlation coefficient is greater than 0.35, to assure the fit is good except for the time delay. Figure 14 shows the obtained time shift for each path and the respective station azimuth in a polar diagram.

In the Grenville Province, we observe total time shifts larger than 1 s in three out of six paths. These are found at north–south and southeast–northwest azimuths. The north–south azimuth path runs along the Appalachian–Grenville boundary, and the observed time shifts are likely related with the velocity contrasts between the two provinces. The cross correlation is more sensitive to the large amplitude features of the waveform, so the time lag usually reflects time shifts of the optimum fit of surface waves. The synthetic *S*-wave arrival for the three paths with estimated time shifts larger than 1 s coincide with the recorded one, but the surface-wave peak is slightly shifted, giving rise to a time lag that does not translate into anisotropy.

In the Appalachian Province, we observe four paths with total time shifts larger than 2 s. To avoid time-lag measurement inconsistencies, we also determine the tangential component time delay by shifting the synthetic waveforms until it fits the *S*-wave and surface-wave arrival times. We do this for the five Appalachian paths with the largest time shifts as shown in Figure 15. We find that the time-shift results of both approaches agree within ± 0.3 s, so we can use the time-lag estimates. The total shift of *S*-arrival estimates, Δt, vary from 0.7 s (QUA2: 270 km, 156°) to 3.5 s (BRY: 336 km, 148°), indicating a significant and consistent delay that is not directly proportional to epicentral distance (although the stations are all within 270–335 km away) but may be related to azimuth. The largest time shifts are observed between 139° and 150° of azimuth. QUA2, which has the smallest shift, is 70 km east of HRV. We estimate the anisotropy percentage using $[2\Delta t/(\Delta t + 2t_d)] \times 100$, where t_d is the arrival time of the recorded tangential *S* wave. The formula is derived from $\{(v_d - v_m)/[(v_d + v_m)/2]\} \times 100$, where v is the *S*-wave velocity and the indices depict data (d) and model (m). We assume that the tangential data and synthetic records are representative of the fast and slow waves, respectively. We obtain an average 2.8% anisotropy for the wave paths within 139° and 156° of azimuth and 3.2% anisotropy if we further limit the azimuth interval to be between 139° and 149°, which removes from the average the path with the lowest time delay (to station QUA2). Table 4 shows the source-to-site azimuth, epicentral distance, time delay, and anisotropy percentage estimates for the five stations in the Appalachian Province with a noticeable delay. There is no simple correlation between local geology or velocity model (h5 and App1) and the pattern of the time lags we observe.

The time delays we obtain are consistent with those reported as part of the mainshock moment tensor inversion reported by Seeber *et al.* (2002) for the same azimuth. In the moment tensor inversion, the filtered waveforms (between 0.03 and 0.1 Hz) are time shifted to produce the maximum correlation with the filtered synthetics. Seeber *et al.* (2002) report time shifts between the vertical and tangential waveforms between 0 and 0.2 s for the paths toward two stations (LBNH and AAM) that each have the azimuth perpendicular to the strike of the fault and time shifts between 1 and 2 s for the paths toward several stations (HRV, KAPO, SCHQ, and A11) that each have azimuths within 45° of the strike of the fault.

Our sensitivity test results show that the surface waves do not sample the mantle space, being insensitive to seismic-velocity variations in the mantle. So, the observed *S*-wave and surface-wave delays of 2.0–3.0 s are indicative of crustal anisotropy. Crustal anisotropy is often associated with one of three features (Babuska and Cara, 1991): the preferential orientation of mineral crystals and tectonic fabric due to deformation; the preferential alignment of microcracks and/or pore spaces (with or without fluid saturation) due to the stress field; and the stratification of isotropic alternating layers with high and low velocities. The tectonic fabric orientation gradually varies from northeast–southwest to the north through north–south to the south of the region. It is within uncertainties and variation of the direction required to fit our results. The spatial variation can explain the lack of a simple pattern of time delays in our data. The orientation of the maximum compressional stress also varies throughout the

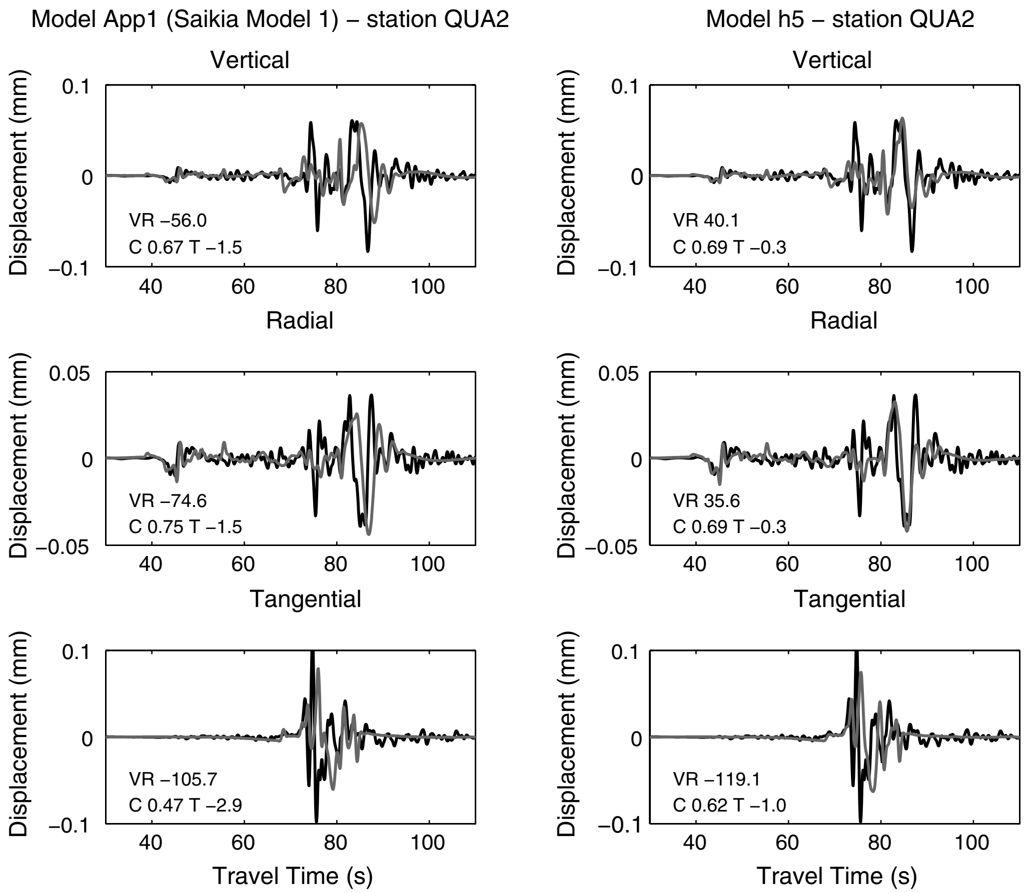

Figure 11. Comparison of the recorded data (black line) with the synthetic seismograms (gray) generated for the path toward station QUA2 (Belchertown, Massachusetts) using App1 and h5 models for the Appalachian Province. The source is convolved in the synthetics. Seismograms are band-pass-filtered between 0.03 and 1 Hz. The numbers in the lower left corner indicate: VR, variance reduction; C, correlation coefficient; and T, time lag in seconds.

Table 2
Average Misfit Values Obtained for Each Modeled Path in the Appalachian Province with h5 and App1 Models*

	h5 Model			App1 Model		
Station	VR	C.Coef	T. Lag (s)	VR	C.Coef	T. Lag (s)
LBNH	−131.7	0.697	1.3	**−58.2**	**0.700**	**0.8**
WVL	−103.0	0.560	1.7	**−30.6**	**0.590**	**4.8**
HRV	−123.4	0.673	1.0	**−80.5**	**0.733**	**1.0**
WES	−64.6	0.680	1.3	**−48.4**	**0.787**	**1.2**
BCX	−80.1	0.597	1.8	**−87.6**	**0.663**	**1.0**
QUA2	**−14.5**	**0.667**	**0.5**	−78.8	0.630	2.0
BRY	**−85.4**	**0.503**	**1.8**	−65.0	0.490	1.8
YLE	**−8.9**	**0.487**	**1.8**	−7.9	0.387	4.4
HNH	**−0.1**	**0.613**	**0.3**	−0.9	0.583	0.7
MNT	**17.0**	**0.637**	**2.4**	2.9	0.653	2.6
Average	**−59.4**	**0.611**	**1.4**	**−45.5**	**0.622**	**2.0**
Low pass	−19.8	0.813	3.9	−37.3	0.817	3.3

	Combined Models—h5 with App1		
	VR	C.Coef	T lag (s)
Average	**−39.7**	**0.638**	**1.6**
Low pass	−29.4	0.820	3.4

*VR, variance reduction; C.Coef, correlation coefficient; T.Lag, absolute time lag.

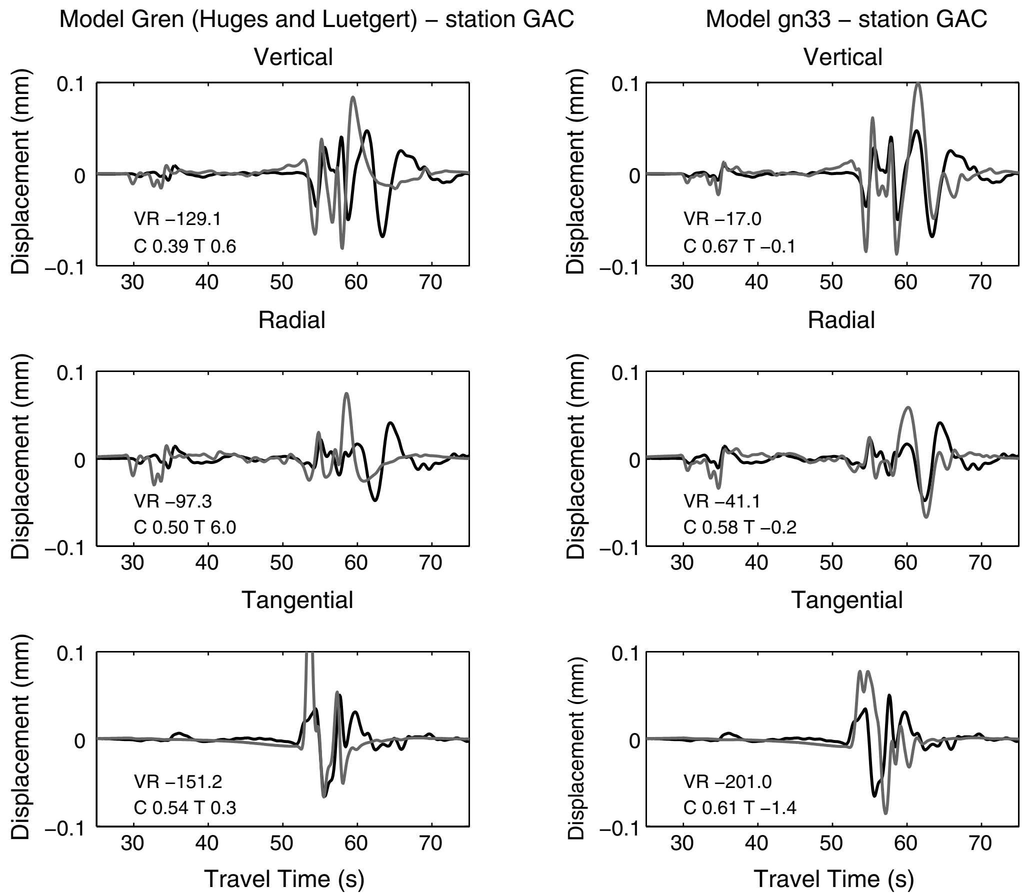

Figure 12. Comparison of the recorded data (black line) with the synthetic seismograms (gray) generated for the path toward station GAC using the Gren and gn33 models for the Grenville Province. The source is convolved in the synthetics. Seismograms are band-pass-filtered between 0.03 and 1 Hz. The numbers in the lower left corner indicate: VR, variance reduction; C, correlation coefficient; and T, time lag in seconds.

region (Yang and Aggarwal, 1981). However, in the crust sampled by our large time-delay paths, the maximum compressional stress is oriented parallel to the ray paths, so the crack orientation will be approximately parallel to the ray paths and hence should be the slow direction (Crampin and Peacock, 2008), which is opposite to our observations. As a result, we prefer the interpretation of anisotropy caused by tectonic fabric.

Table 3
Average Misfit Values Obtained for Each Modeled Path in the Grenville Province with gn33 and Gren Models*

	gn33			Gren		
Station	VR	C.Coef	T.Lag (s)	VR	C.Coef	T.Lag (s)
ACCN	−21.6	0.700	0.9	−50.4	0.717	0.9
BINY	1.8	0.610	0.8	−82.8	0.417	6.6
CONY	−6.4	0.693	0.6	−56.5	0.653	0.8
GAC	−86.4	0.620	0.6	−125.9	0.477	2.3
KGNO	13.2	0.767	0.3	−113.9	0.677	1.3
NCB	11.5	0.787	0.2	−74.5	0.777	0.8
Average	**−12.0**	**0.696**	**0.6**	**−84.0**	**0.619**	**2.2**
Low pass	−217.7	0.832	3.5	−137.9	0.827	3.4

*VR, variance reduction; C.Coef, correlation coefficient; T.Lag, absolute time lag.

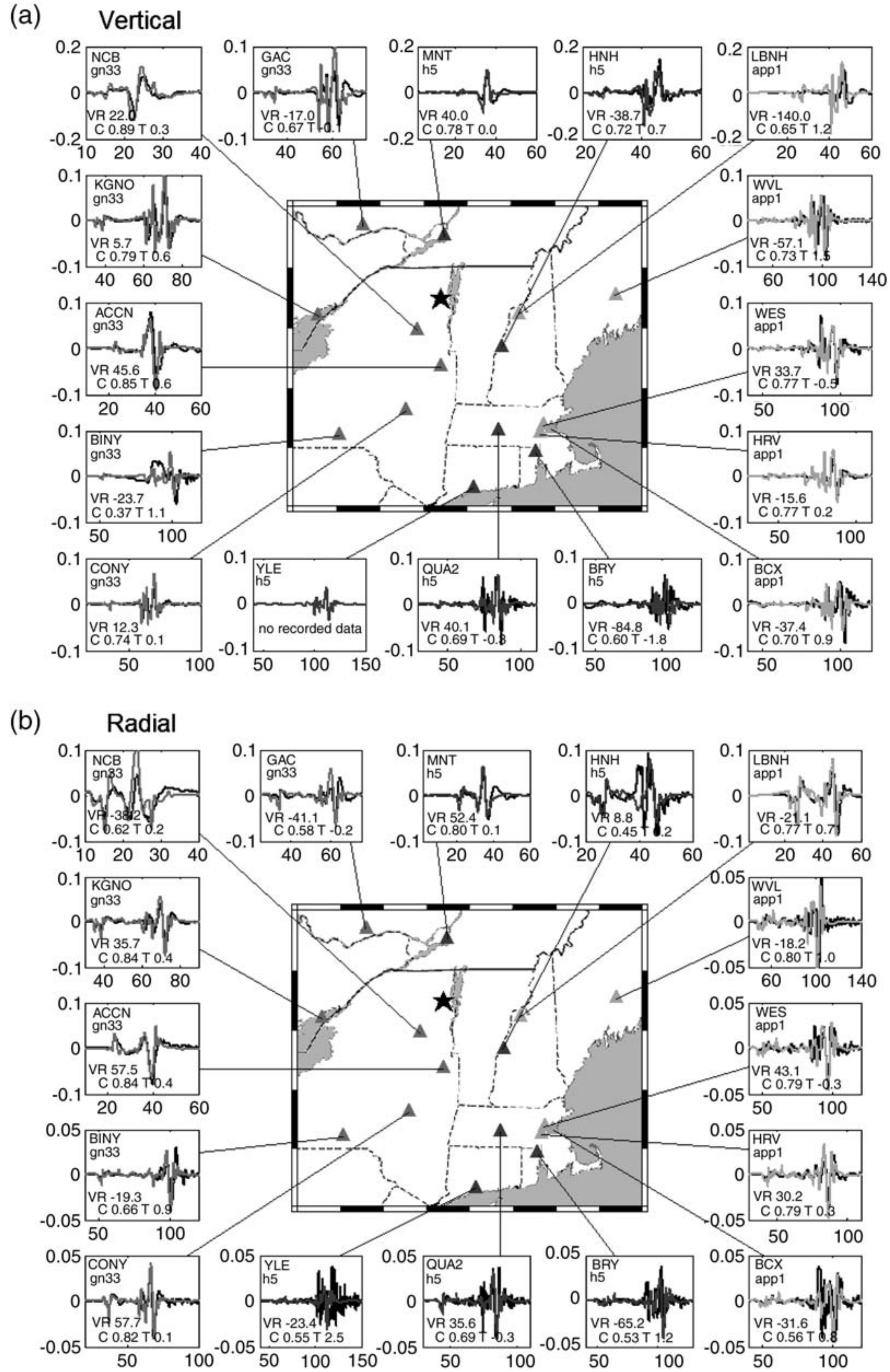

Figure 13. (a) Map showing the stations used in this study and comparing the vertical component of the recorded and synthetic data computed with the preferred models for each source-station paths. Synthetics generated with models gn33 are shown in gray, with h5 in dark gray, and with App1 in light gray. Recorded data are displayed in black. Seismograms are filtered between 0.03 and 1 Hz. The numbers in the lower left corner indicate: VR, variance reduction; C, correlation coefficient; and T, time lag in seconds. The star indicates the Au Sable Fork earthquake epicenter location. (b) Same as (a) but for radial component. (c) Same as for (a) but for tangential component. (*Continued*)

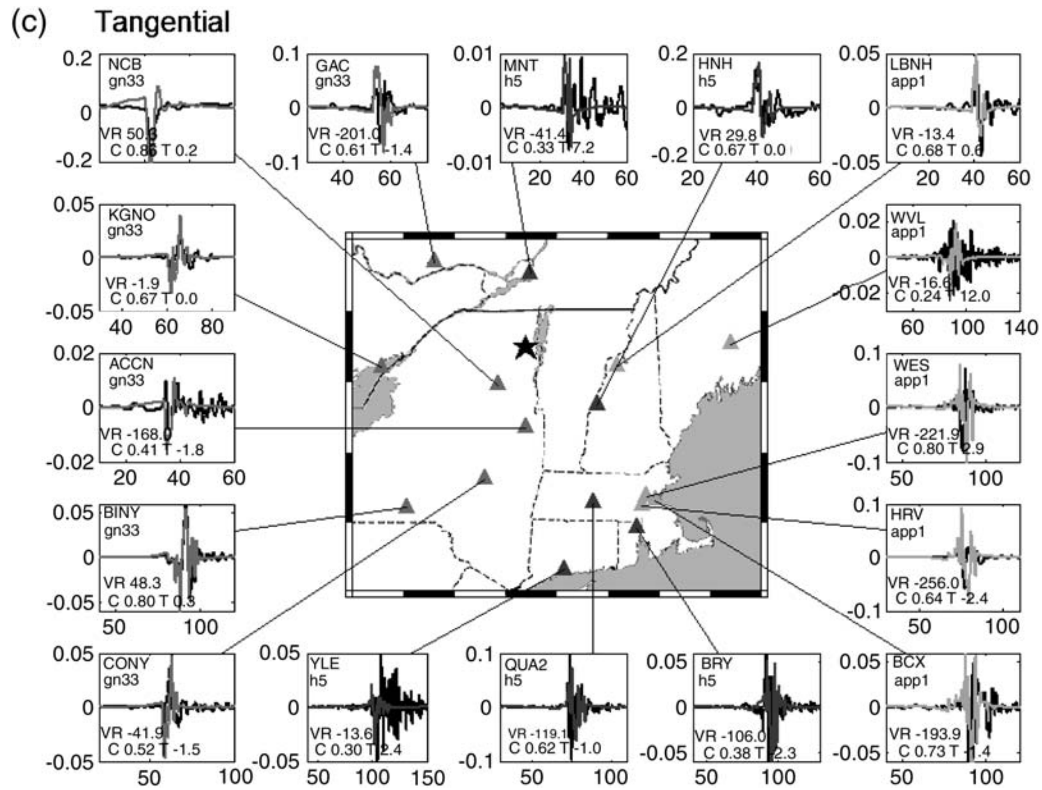

Figure 13. Continued.

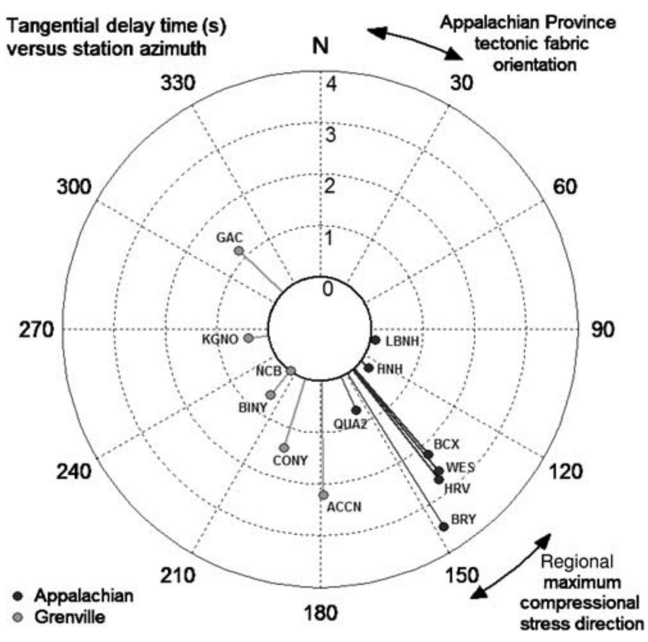

Figure 14. Anisotropy polar diagram. Tangential-component delay time versus station azimuth. The delay time is estimated from the tangential minus radial time lags (obtained from the cross correlation) to remove any time delay introduced by the velocity model. Black and gray represent Appalachian and Grenvillian paths, respectively. Paths for which the tangential correlation coefficient is smaller than 0.35 are not plotted. The small interior circle represents 0 s delay.

Conclusions

The Au Sable Forks earthquake is the largest earthquake to be recorded in NEUS by multiple broadband stations. The data recorded at these stations enables us to test, validate, and refine the existing 1D regional crustal models, which were developed with very limited data. We test several published 1D velocity models for the Appalachian and Grenville Provinces in order to validate and choose a best-fit model for each province. We use a combination of qualitative and quantitative goodness-of-fit measures to compare synthetic seismograms with observed ground motions. The best-fit 1D crustal model for each province is then used as an initial model for a sensitivity analysis and forward modeling of incrementally adjusted crustal-velocity models. We use the Saikia (1994) model 1 (App1) for the Appalachian Province and the Hughes and Luetgert (1991) model (Gren) for the Grenville Province. We perform sensitivity tests on both models in order to understand the effect of changes in 1D structure on the waveforms.

For the Grenville Province, our sensitivity analyses indicate that the Gren model is improved with slightly slower P-wave velocities (~2%) and with a thicker crust. Our sensitivity analysis also indicates that the synthetic ground motions could be better matched to the observed ground motions at higher frequencies (< 1 Hz) with refinement of the surface layers in the velocity models. The Gren model is very simple, with only a single 0.5-km surface layer.

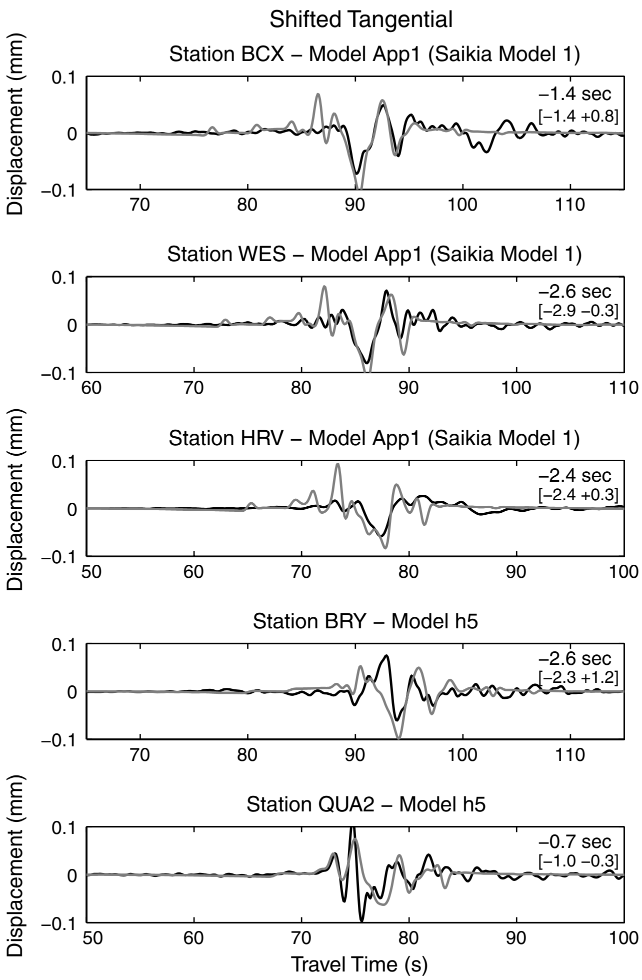

Figure 15. Anisotropy. Tangential component generated with the preferred models (App1 or h5) for the paths toward the stations QUA2, WES, HRV, BCX, and BRY in the Appalachian Province. Black line is the recorded data, and gray lines are the synthetics. The synthetics are shifted in time to better fit the data. Numbers on the top right corner represent the time (in seconds) that the seismograms were shifted; negative values mean they were anticipated in time. The time lags obtained from the cross correlation between the data and the synthetics are shown in brackets for the tangential and radial component, respectively.

We develop model gn33 with a three-layer gradient in the upper 3 km, which shows improvements for the average of all the modeled source-station paths.

For the Appalachian Province, the App1 model has a detailed five-layer gradient in the upper 5 km. The sensitivity analysis showed that the Moho depth and intermediate layers modeled the arrivals well and did not contribute significantly to the misfit. It also showed that the contribution of the mantle gradient in the App1 model is insignificant, as expected for the wave paths at epicentral distances less than 400 km used in this study. We develop model h5 with a single 3 km surface layer and constant mantle velocities, which fits the data somewhat better at five out of ten stations in the Appalachian Province.

We propose/recommend the 1D velocity models App1/h5 and gn33 for modeling wave propagation in the Appalachian and Grenville Provinces, respectively, at intermediate frequencies (up to 1 Hz). We find an average increase of P-wave and S-wave velocity of ~2% for the Grenville Province (0.1 km/s for P waves and of 0.05 km/s for S waves) when comparing the crustal velocity profiles of the two provinces.

Our analysis of the regional wave field resulting from the Au Sable Forks earthquake identified several potential complexities that could not be accounted for in simple 1D crustal models and therefore merit further study with new data: (1) We observe anisotropy between SH and SV for the paths toward the stations at 140°–150° of azimuth (WES, BRY, HRV, BCX, and QUA2), resulting in delays in the synthetics on the order of 1–3 s. Based on the time-delay measurements, we estimate 3% anisotropy for wave paths along this azimuth direction, which is parallel to the direction of the regional maximum compressional stress and has a low angle to the regional tectonic fabric. (2) We observe complex tangential ground shaking at the three stations (MNT, ACCN, and YLE) located along the boundary between the Appalachian and Grenville Provinces. The late-arriving energy in these records is likely related to complex wave paths through the Grenvillian Ramp zone and associated structures.

Data and Resources

The facilities of the Incorporated Research Institutions for Seismology Data Management System (IRIS DMS), and specifically the IRIS Data Management Center, were used for access to the waveform and metadata required in

Table 4
Anisotropy Percentage Estimates for Stations in the Appalachian Province with a Noticeable Synthetic Time Delay

			Synthetic Delay Time (s)			
Station	Epicentral Distance (km)	Source-to-Site Azimuth (°)	Difference between Tangential and Radial (Tangential–Radial)	Tangential	Radial	Anisotropy (%)
BCX	314.7	139.1	2.2	1.4	−0.8	2.4
WES	302.6	140.3	2.6	2.9	0.3	3.1
HRV	280.0	141.7	2.7	2.4	−0.3	3.5
BRY	335.5	148.2	3.5	2.3	−1.2	3.8
QUA2	269.3	156.2	0.7	1.0	0.3	1.0

this study. The IRIS DMS is funded through the National Science Foundation and specifically the Geoscience Directorate through the Instrumentation and Facilities Program of the National Science Foundation under cooperative agreement EAR-0552316. Seismograms used in this study were also collected using the Earthquakes Canada (Geological Survey Canada, Continuous Waveform Archive, AutoDRM@seismo.NRCan.gc.ca, Natural Resources Canada [http://earthquakescanada.nrcan.gc.ca/cite-eng.php, last accessed September 2008]), and the New England Seismic Network (NESN) at Weston Observatory/Boston College. Some data processing was made using the Seismic Analysis Code (Goldstein *et al.*, 2003). Figures 1 and 13 were made using Generic Mapping Tools, version 4.2.1 (www.soest.hawaii.edu/gmt; Wessel and Smith, 1998).

Acknowledgments

We are grateful to W.-Y. Kim for providing us with information about his study of the Au Sable Forks aftershock sequence and to J. Ristau for his helpful comments on the moment tensor method. The comments of D. Heaton, M. Chapman, and two anonymous reviewers greatly improved this manuscript. This research is sponsored by the U.S. Geological Survey, Department of the Interior, External Grant Award numbers 04HQGR0166 and 04HQGR0167. The views and conclusions contained in this document are those of the authors and should not be interpreted as necessarily representing the official policies, either expressed or implied, of the U.S. government.

References

Abercrombie, R. E., and J. R. Rice (2005). Small earthquake scaling revisited: Can it constrain slip weakening?, *Geophys. J. Int.* **162,** 406–424.

Atkinson, G. M. (1989). Implications of eastern ground-motion characteristics for seismic hazard assessment in eastern North America, *Ann. New York Acad. Sci.* **558,** 128–135.

Atkinson, G. M., and D. M. Boore (1995). Ground-motion relations for eastern North America, *Bull. Seismol. Soc. Am.* **85,** no. 1, 17–30.

Atkinson, G. M., and D. M. Boore (1998). Evaluation of models for earthquake source spectra in eastern North America, *Bull. Seismol. Soc. Am.* **88,** no. 4, 917–934.

Atkinson, G. M., and D. M. Boore (2006). Earthquake ground-motion prediction equations for eastern North America, *Bull. Seismol. Soc. Am.* **96,** 2181–2205.

Atkinson, G. M., and E. Sonley (2003). Ground motions from the 2002 Au Sable Forks, New York earthquake of M 5.0, *Seismol. Res. Lett.* **74,** no. 3, 339–349.

Babuska, V., and M. Cara (1991). *Seismic Anisotropy in the Earth*, Kluwer Academic Publishers, Dordrecht, The Netherlands.

Baig, A. M., F. A. Dahlen, and S.-H. Hung (2003). Travel times of waves in three-dimensional random media, *Geophys. J. Int.* **153,** 467–482.

Baise, L. G., D. S. Dreger, and S. D. Glaser (2003). Modeling of the northern San Francisco Bay velocity structure for the 18 August 1999 Bolinas earthquake, *Bull. Seismol. Soc. Am.* **93,** no. 1, 465–479.

Campbell, K. (2003). Prediction of strong ground motion using the hybrid empirical method and its use in the development of ground-motion (attenuation) relations in eastern North America, *Bull. Seismol. Soc. Am.* **93,** no. 3, 1012–1033.

Chi, W.-C., D. S. Dreger, and A. Kaverina (2001). Finite source modeling of the 1999 Taiwan (Chi-Chi) earthquake derived from a dense strong-motion network, *Bull. Seismol. Soc. Am.* **91,** 1144–1157.

Crampin, S., and S. Peacock (2008). A review of the current understanding of shear-wave splitting in the crust and common fallacies in interpretation, *Wave Motion* **45,** 675–722.

Detweiler, S., and W. D. Mooney (2003). The relation of the Grenville/Appalachian boundary to the April 20, 2002 Au Sable Forks, New York and the April 29, 2003 Fort Payne, Alabama earthquakes, *Eos Trans. AGU* **84,** no. 46, Fall Meeting Suppl., Abstract S21E-0348.

Dreger, D. S., and D. V. Helmberger (1990). Broadband modeling of local earthquakes, *Bull. Seismol. Soc. Am.* **80,** 1162–1179.

Dreger, D. S., and D. V. Helmberger (1993). Determination of source parameters at regional distances with three-component sparse network data, *J. Geophys. Res.* **98,** 8107–8125.

Du, W.-X., W.-Y. Kim, and L. R. Sykes (2003). Earthquake source parameters and state of stress for the northeastern United States and southeastern Canada from analysis of regional seismograms, *Bull. Seismol. Soc. Am.* **93,** no. 4, 1633–1648.

Eaton, D. W., S. Dineva, and R. Mereu (2006). Crustal thickness and V_P/V_S variations in the Grenville orogen (Ontario, Canada) from analysis of teleseismic receiver functions, *Tectonophysics* **420,** 223–238.

Eshelby, J. D. (1957). The determination of the elastic field of an ellipsoidal inclusion and related problems, *Proc. Roy. Soc. Lond. A* **241,** 376–396.

Frankel, A., A. McGarr, J. Bicknell, J. Mori, L. Seeber, and E. Cranswick (1990). Attenuation of high-frequency shear waves in the crust: Measurements from New York state, South Africa, and southern California, *J. Geophys. Res.* **95,** no. B11, 17441–17457.

Frankel, A., C. Mueller, T. Barnhard, D. Perkins, E. V. Leyendecker, N. Dickman, S. Hanson, and M. Hopper (1996). National seismic hazard maps: Documentation June 1996, *U.S. Geological Survey Open-File Report 96-532*.

Frankel, A. D., M. D. Petersen, C. S. Mueller, K. M. Haller, R. L. Wheeler, E. V. Leyen-decker, R. L. Wesson, S. C. Harmsen, C. H. Cramer, D. M. Perkins, and K. S. Rukstales (2002). Documentation for the 2002 update of the national seismic hazard maps, *U.S. Geological Survey Open-File Report 02-420*, 33 pp., available at http://pubs.usgs.gov/of/2002/ofr-02-420/OFR-02-420.pdf (last accessed May 2010).

Goldstein, P., D. Dodge, M. Firpo, and L. Minner (2003) SAC2000: Signal processing and analysis tools for seismologists and engineers, invited contribution to *The IASPEI International Handbook of Earthquake and Engineering Seismology*, W. H. K. Lee, H. Kanamori, P. C. Jennings, and C. Kisslinger (Editors), Academic Press, London.

Hartzell, S. H. (1978). Earthquake aftershocks as Green's functions, *Geophys. Res. Letters* **5,** 1–4.

Helmberger, D. V., L. S. Zhao, D. S. Dreger, and V. Lefevre (1992). Exploration of the lower lithosphere: Northeastern United States, *Phys. Earth Planet. In.* **70,** no. 1–2, 22–38.

Hines, E. M., L. G. Baise, and S. S. Swift (2010). Ground motion suite selection for eastern North America, *J. Struct. Eng.* available at http://dx.doi.org/10.1061/(ASCE)ST.1943-541X.0000258 (last accessed July 2010).

Hughes, S., and J. H. Luetgert (1991). Crustal structure of the western New England Appalachians and the Adirondack Mountains, *J. Geophys. Res.* **96,** 16471–16494.

Hughes, S., and J. H. Luetgert (1992). Crustal structure of the southeastern Grenville province, northern New York and Eastern Ontario, *J. Geophys. Res.* **97,** 17455–17479.

Hughes, S., J. H. Luetgert, and N. I. Christensen (1993). Reconciling deep seismic refraction and reflection data from the Grenvillian-Appalachian boundary in western New England, *Tectonophysics* **225,** no. 4, 255–269.

Kanamori, H., and D. L. Anderson (1975). Theoretical basis of some empirical relations in seismology, *Bull. Seismol. Soc. Am.* **65,** no. 5, 1073–1095.

Kim, W.-Y., and R. E. Abercrombie (2006). Source scaling of earthquakes in the northeastern United States: Collaborative research with Columbia University and Boston University, *NEHRP Final Technical Report*, Award Number 04HQGR-0028, 19 pp.

Kim, A., D. S. Dreger, and S. Larsen (2010). Moderate earthquake ground-motion validation in the San Francisco Bay area, *Bull. Seismol. Soc. Am.* **100,** no. 2, 819–825.

Kim, W.-Y., L. Seeber, and J. G. Armbruster (2002). Source process of the M_w 5.0 Au Sable Forks, New York earthquake from local aftershock monitoring network data, *Eos Trans. AGU* **83,** no. 47, Fall Meet. Suppl., Abstract S22D-01.

Levin, H. L. (2006) *The Earth Through Time*, eighth ed., John Wiley & Sons, Inc, New York, 560 pp.

Levin, V., W.-Y. Kim, and W. Menke (1995). Seismic velocities in the shallow crust of western New England and northern New York, *Bull. Seismol. Soc. Am.* **85,** no. 1, 207–219.

Li, A., D. W. Forsyth, and K. M. Fischer (2003). Shear velocity structure and azimuthal anisotropy beneath eastern North America from Rayleigh wave inversion, *J. Geophys. Res.* **108,** no. B8, 2362, doi 10.1029/2002JB002259.

Ma, S., and G. M. Atkinson (2006). Focal depths for small to moderate earthquakes ($m_N \geq 2.8$) in western Quebec, southern Ontario, and northern New York, *Bull. Seismol. Soc. Am.* **96,** no. 2, 609–623.

Madariaga, R. (1976). Dynamics of an expanding circular crack, *Bull. Seismol. Soc. Am.* **66,** 639–666.

Mareschal, J. C., and C. Jaupart (2004). Variations of surface heat flow and lithospheric thermal structure beneath the North American craton, *Earth Planet. Sci. Lett.* **223,** 65–77.

Musacchio, G., W. D. Mooney, J. H. Luetgert, and N. I. Christensen (1997). Composition of the crust in the Grenville and Appalachian Provinces of North America inferred from V_P/V_S ratios, *J. Geophys. Res.* **102,** 15225–15242.

Olsen, K. B. (2000). Site amplification in the Los Angeles basin from 3D modeling of ground motion, *Bull. Seismol. Soc. Am.* **90,** S77–S94.

Peterson, M. D., A. D. Frankel, S. C. Harmsen, C. S. Mueller, K. M. Haller, R. L. Wheeler, R. L. Wesson, Y. Zeng, O. S. Boyd, D. M. Perkins, N. Luco, E. H. Field, C. J. Wills, and K. S. Rukstales (2008). Documentation for the 2008 update of the United States national seismic hazard maps, *USGS Open File Report 2008-1128*, 128 pp., available at http://pubs.usgs.gov/of/2008/1128/pdf/OF08-1128_v1.1.pdf (last accessed May 2010).

Pitarka, A., R. Graves, and P. Somerville (2004). Validation of a 3D velocity model of the Puget Sound region based on modeling ground motion from the 28 February 2001 Nisqually earthquake, *Bull. Seismol. Soc. Am.* **94,** 1670–1689.

Saikia, C. K. (1994). Modified frequency–wavenumber algorithm for regional seismograms using Filon's quadrature: Modelling of *Lg* waves in eastern North America, *Geophys. J. Int.* **118,** 142–158.

Seeber, L., W.-Y. Kim, J. G. Armbruster, W.-X. Du, and A. Lerner-Lam (2002). The 20 April 2002 M_w 5.0 earthquake near Au Sable Forks, Adirondacks, New York: A first glance at a new sequence, *Seismol. Res. Lett.* **73,** 480–489.

Shi, J., W.-Y. Kim, and P. G. Richards (1996). Variability of crustal attenuation in the northeastern United States from *Lg* waves, *J. Geophys. Res.* **101,** 25231–25242.

Silva, W., N. Gregor, and R. Darragh (2002). Development of hard rock attenuation relations for central and eastern North America, , internal report from Pacific Engineering, 1 November 2002, available at http://www.pacificengineering.org/CEUS/Development%20of%20Regional%20Hard_ABC.pdf (last accessed May 2010).

Sipkin, S. A. (1982). Estimation of earthquake source parameters by the inversion of waveform data: Synthetic waveforms, *Phys. Earth Planet. In.* **30,** 242–259.

Somerville, P. (1989). Earthquake source and ground-motion characteristics in eastern North America, *Ann. New York Acad. Sci.* **558,** 105–127.

Somerville, P., N. Collins, N. Abrahamson, R. Graves, and C. Saikia (2001). Earthquake source scaling and ground motion attenuation relations for the central and eastern United States, *Final Report to the U.S. Geological Survey*, Contract No. 99HQGR0098; available at http://earthquake.usgs.gov/research/external/reports/99HQGR0098.pdf (last accessd May 2010).

Stidham, C., M. Antolik, D. Dreger, S. Larsen, and B. Romanowicz (1999). Three-dimensional structure influences on the strong motion wavefield of the 1989 Loma Prieta earthquake, *Bull. Seismol. Soc. Am.* **89,** 1184–1202.

Tavakoli, B., and S. Pezeshk (2005). Empirical-stochastic ground-motion prediction for eastern North America, *Bull. Seismol. Soc. Am.* **95,** 2283–2296.

Taylor, S. R., M. N. Toksoz, and M. P. Chaplin (1980). Crustal structure of the northeastern United States: Contrasts between Grenville and Appalachian Provinces, *Science* **208,** 595–597.

Toro, G., N. Abrahamson, and J. Schneider (1997). Model of strong motion in eastern and central North America: Best estimates and uncertainties, *Seismol. Res. Lett.* **68,** 41–57.

U.S. Geological Survey (USGS) (2002). Magnitude 5.2 NEW YORK 2002 April 20 10:50:47 UTC, Preliminary Earthquake Report, *USGS Earthquake Hazards Program: Earthquake Report: New York*, available at http://neic.usgs.gov/neis/eq_depot/2002/eq_020420/ (last accessed may 2010).

Viegas, G., R. E. Abercrombie, and W.-Y. Kim (2010). The 2002 *M* 5 Au Sable Forks, NY, earthquake sequence: Source scaling relationships and energy budget, *J. Geophys. Res.*, doi 10.1029/2009JB006799 (in press).

Wald, D. J., and R. W. Graves (1998). The seismic response of the Los Angeles basin, California, *Bull. Seismol. Soc. Am.* **88,** 337–356.

Wessel, P., and W. H. F. Smith (1998). New, improved version of generic mapping tools released, *EOS Trans. AGU* **79,** 579.

Wheeler, R. L. (1995). Earthquakes and the cratonward limit of Iapetan faulting in eastern North America, *Geology* **23,** 105–108.

Yang, J. P., and Y. P. Aggarwal (1981). Seismotectonics of the northeastern United States and adjacent Canada, *J. Geophys. Res.* **86,** 4981–4998.

Zhao, L. S., and D. V. Helmberger (1991). Broad-band modeling along a regional shield path, Harvard recording of the Sanguenay earthquake, *Geophys. J. Int.* **105,** no. 2, 301–312.

Zhu, H., and J. E. Ebel (1994). Tomographic inversion for the seismic velocity structure beneath northern New England using seismic refraction data, *J. Geophys. Res.* **99,** 15331–15357.

Department of Earth Sciences
Boston University
685 Commonwealth Avenue
Boston, Massachusetts 02215
gisofer@gmail.com
rea@bu.edu
(G.M.V., R.E.A.)

Department of Civil and Environmental Engineering
Tufts University
113 Anderson Hall
Medford, Massachusetts 02155
laurie.baise@tufts.edu
(L.G.B.)

Manuscript received 24 January 2007